# SEARCH FOR THE DIRECT DECAY MODES $K^+ \to \mu^+ + \nu + \gamma$ AND $K^+ \to \pi^+ + \gamma + \gamma$

Min Chen
(Ph. D. Thesis)

January 1969



LRL
LAWRENCE RADIATION LABORATORY
UNIVERSITY of CALIFORNIA BERKELEY

UCRL-18653
c.2 rev.

## DISCLAIMER

UCRL-18653

UNIVERSITY OF CALIFORNIA

Lawrence Radiation Laboratory
Berkeley, California

AEC Contract No. W-7405-eng-48

# SEARCH FOR THE DIRECT DECAY MODES $K^+ \to \mu^+ + \nu + \gamma$ AND $K^+ \to \pi^+ + \gamma + \gamma$

Min Chen

(Ph. D. Thesis)

January 1969

(III) Appendices

# SEARCH FOR THE DIRECT DECAY MODES $K^+ \to \mu^+ + \nu + \gamma$ AND $K^+ \to \pi^+ + \gamma + \gamma$

Min Chen

Lawrence Radiation Laboratory
University of California
Berkeley, California

January 1969

ABSTRACT

I. Search for the Direct Decay $K^+ \to \mu^+ + \nu + \gamma$

We searched for the direct decay $K^+ \to \mu^+ + \nu + \gamma$ as part of our stopping $K^+$ spark chamber experiment at the Bevatron. The direct decay is experimentally distinguished from ordinary inner bremsstrahlung by a measurement of the angle $\theta$ between the direction of the muon and gamma ray emission for events with high energy muons. The direct decay favors the emission of photons in a direction opposite to that of energetic muons while for the inner bremsstrahlung the emission of soft photons at small forward angle prevails.

We found 27 events with muon kinetic energy between 137 and 142 MeV. Each of the selected 27 events was associated with a converted gamma ray shower. None of these events have the angle $\theta$ in the interval $-1 < \cos\theta < -0.9$ where more than 66% of the direct decay $K^+ \to \mu^+ + \nu + \gamma$ events should appear. The upper limit for the branching ratio of the direct decay of $K^+ \to \mu^+ + \nu + \gamma$ in the above muon spectrum interval is $1.1 \times 10^{-5}$ at 90% confidence level. If we assume that the E1 decay amplitude is negligible, we can set an upper limit on the M1 form factor ($h_M$) of 2.3 at 95% confidence level.

## A. INTRODUCTION

The matrix element for $K^+ \rightarrow \mu^+ + \nu + \gamma$ can be divided into two terms,

$$M = M_b + M_s$$

$M_b$ is the contribution of ordinary inner bremsstrahlung while $M_s$ includes all the processes in which the gamma ray is emitted directly. This latter term is also referred to as the structure term as it is determined by the internal structure of the K meson. The calculation of the structure term is complicated, so it is necessary to assume a detailed model of the process in order to estimate its magnitude.

If time reversal invariance is valid the phase difference between $M_b$ and $M_s$ is zero. In the convention which we employ in this paper $M_b$ is real. Time reversal invariance therefore requires the form factors which describe $M_s$ to be real. The experimental consequences of a T violation will appear as a component of the polarization of the muon out of the plane containing the $\mu$, $\nu$, and $\gamma$ momenta.

It was suggested[1,3,4] that there may be an appreciable violation of time reversal invariance in processes such as $K^+ \rightarrow \mu^+ + \nu + \gamma$. Unless the absolute value of $M_s$ is comparable with that of $M_b$--at least for some kinematic configuration--it will not be possible to design practical experiments in which the time reversal violation would be detectable. For the experiment we describe in this paper, we have set a limit on the magnitude of $M_s$.

The inner-bremsstrahlung term has been calculated by Cabibbo[2] in the case of $\pi^+ \rightarrow \mu^+ + \nu + \gamma$. This calculation applies also to $K^+ \rightarrow \mu^+ + \nu + \gamma$. According to V-A theory, the matrix element responsible

for the decay $K^+ \to \mu^+ + \nu$ is

$$M = \frac{G f_K}{\sqrt{4p_o}} p_\mu \bar{U}_\ell \gamma_\mu (1+\gamma_5) U_\nu$$

where $p_\mu$ is the four momentum of the $K^+$ meson and $\gamma_\mu$ are the Dirac $\gamma$ matrices; G is the weak interaction coupling constant; $f_K$ is a constant; and $\bar{U}_\ell$ and $U_\nu$ are the spinors of the muon and the neutrino respectively. By making the usal assumption of a minimal electromagnetic interaction, and by assuming that the weak interaction form factors are constant and equal to their on-mass-shell values, the inner bremsstrahlung matrix element $M_b$ can be calculated in a straightforward fashion. The gauge-invariant matrix element for inner bremsstrahlung is:

$$M_b = ie \frac{f_K G m_\mu}{\sqrt{2}\sqrt{4p_o k_o}} \bar{U}_\ell \left[ \frac{\ell\cdot\epsilon}{\ell\cdot k} - \frac{p\cdot\epsilon}{p\cdot k} + \frac{\epsilon\cdot\gamma\ k\cdot\gamma}{2\ell\cdot k} \right] (1+\gamma_5) U_\nu \ . \quad \text{(I-1)}$$

where $e^2$ is the fine structure constant, $e^2 = \frac{4\pi}{137}$, $\ell_\mu$, $k_\mu$, and $\epsilon_\mu$ are the four momentum of the $\mu$ meson and the four momentum and polarization of the gamma; A·B is defined as $A_o B_o - \vec{A}\cdot\vec{B}$. The direct matrix $M_s$ is difficult to calculate. From Lorentz invariance, gauge invariance and (V-A) theory the most general form of the direct matrix element for the decay $K^+ \to \mu^+ + \nu + \gamma$ is[3]

$$M_s = \frac{ie\ G\ f_K}{\sqrt{2}\sqrt{4p_o k_o}} \bar{U}_\ell \left[ \frac{h_E}{m_K^2} \Big( (p\cdot k)(\epsilon\cdot\gamma) - (\epsilon\cdot p)(k\cdot\gamma) \Big) \right.$$

$$\left. + \frac{h_M}{m_K^2} i\, \epsilon_{\lambda\mu\rho\sigma}\, \gamma_\lambda p_\mu \epsilon_\rho k_\sigma \right] (1+\gamma_5) U_\nu \ . \quad \text{(I-2)}$$

where $\epsilon_{\lambda\mu\rho\sigma}$ = +1 if $\lambda\mu\rho\sigma$ are an even permutation of 0,1,2,3,

$\epsilon_{\lambda\mu\rho\sigma}$ = -1 if they are an odd permutation, and

$\epsilon_{\lambda\mu\rho\sigma}$ = 0 if two or more indices are equal.

$h_E$ and $h_M$ are the form factors for E1 and M1 respectively. They are generally functions of $q^2$, the square of the invariant mass of the lepton pair. In a system where the $K^+$ decays at rest, $q^2 = m^2_K - 2m_K E_\gamma$. As the experiment we are describing here has a limited number of events we shall assume that $h_E$ and $h_M$ are constant and equal to $h_E(E_\gamma=0)$ and $h_M(E_\gamma=0)$ respectively. If indeed they are not, our result must be considered as an average over the spectrum of kinematical configurations. In fact the form factors $h_E$ and $h_M$ have been estimated from a number of theoretical models.[3,4,5] It has been shown[3] that the odd parity strange vector mesons ($1^-$) will contribute to $h_M$ and the even parity strange vector mesons ($1^+$) will contribute to $h_E$. Since the K* has the lowest mass, it is likely that it is the dominant contribution to $M_s$. Gervais et al.[4] used a K*(890 MeV) pole model to calculate the value of $h_M$. All contributions from higher mass states were neglected. Their model can be expressed in the following diagrams:

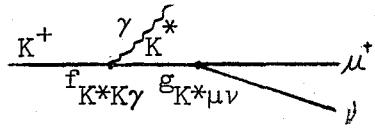


+ (Inner Bremsstrahlung terms)

The matrix element at K*Kγ vertex is

$$H_1 = \frac{1}{2} f_{K^*K\gamma} \epsilon_{\lambda\mu\rho\sigma} F_{\lambda\mu} (K^*)^\dagger_\rho \frac{\partial}{\partial x\sigma} \varphi_K$$

where $f_{K^*K\gamma}$ is the coupling constant, $K^*_\rho$ is the polarization vector of the K* and $F_{\lambda\mu}$ is defined by

$$F_{\lambda\mu} = k_\mu \epsilon_\lambda - k_\lambda \epsilon_\mu$$

and $\varphi_K$ is the K field. The matrix element at the vertex K*μν is

$$H_2 = g_{K^*\mu\nu}(K^*)_\alpha \, \bar{U}_\ell \, \gamma_\alpha(1+\gamma_5)U_\nu \quad .$$

The contribution of the K*-pole term to the decay $K^+ \to \mu^+ + \nu + \gamma$ is

$$H = ie \frac{f_{K^*K\gamma} \, g_{K^*\mu\nu}}{\sqrt{4p_o k_o}} \, \epsilon_{\lambda\mu\rho\sigma} \, k_\sigma \epsilon_\rho P_\mu \bar{U}_\ell \gamma_\lambda (1+\gamma_5) U_\nu \, \frac{1}{(p-k)^2 - m^2_{K^*}} \qquad \text{(I-3)}$$

The coupling constant $f_{K^*K\gamma}$ was related by $SU_6$ to the $\rho\pi\gamma$ coupling constant and the latter was estimated by assuming the $\rho \to \pi + \gamma$ partial width of the order of 0.5 MeV. They got

$$|f_{K^*K\gamma}| = 3.5/m_k$$

However a similar calculation by Jackson[12] using the $SU_6$ relation $f_{K^*K\gamma} = \frac{1}{3} f_{\omega\pi\gamma}$ and the experimental width $\tau(\omega^o \to \pi^o + \gamma) = 1.1$ MeV gives $|f_{K^*K\gamma}| = 0.5/m_K$. The numerical value of $g_{K^*\mu\nu}$ can be related to the $K_{e3}$ partial rate by assuming a K*-pole model. $g_{K^*\mu\nu}$ was estimated to be $1.9 \times 10^{-7}$ by Gervais et al. and to be $3.1 \times 10^{-7}$ by Jackson. Comparing the term of $h_M$ in Eq. (I-2) with that in Eq. (I-3) we find in this model the form factor becomes:

$$h_M = \frac{f_{KK^*\gamma} \, g_{K^*\mu\nu}}{g} \, \frac{m^2_K}{((p-k)^2 - m_{K^*}{}^2)} \quad \text{with} \quad g = \frac{G \, f_K}{\sqrt{2}} = 1.42 \times 10^{-7}/m_K \qquad \text{(I-4)}$$

from which we find $h_M$=2 according to the values estimated by Gervais et al. and $h_M$=0.5 according to Jackson if the dependence on $k_o$ is neglected. The discrepancy between the two values of $h_M$ must apparently be attributed to the different numerical values used as input data.

For comparison, the corresponding $h_M$ in $\pi^{\pm} \to \mu^{\pm}(e^{\pm}) + \nu + \gamma$ mode was estimated[3] to be $\sqrt{3}\times 10^{-2}$ from CVC theory and the life time of $\pi^o$.

The El form factor $h_E$ was estimated[5] to be:

$$h_E = 0.8\, h_M$$

if unsubtracted dispersion relation holds for $h_E(q^2)$ or

$$|h_E| \ll |h_M|$$

if once subtacted dispersion relation holds for $h_E(q^2)$.

The differential distribution in muon energy $E_\mu$ (or $\ell_o$) and cosine of the angle $\theta$ between the muon and photon directions, evaluated in the rest frame of the K meson, is

$$\frac{d^2 W}{dE_\mu\, d\cos\theta} = \frac{W_{K\ell}}{2k_{max}^2} \frac{dL}{d\Omega} (S_o+S_1+S_2) \frac{(m_K^2+2\ell m_K \cos\theta - m_\mu^2 + \frac{1}{\ell}(m_K^2+m_\mu^2-2m_K\ell_o)\ell_o\cos\theta)}{(m_K - \ell_o + \ell\cos\theta)^2} \qquad \text{(I-5)}$$

where

$$S_o = \frac{1}{\ell\cdot k}\left[\ell^2 \sin^2\theta (2m_K k_{max}/\ell\cdot k) + 2\nu\cdot k\right],$$

$$S_1 = \frac{-4}{\ell\cdot k}\left[\ell^2 \sin^2\theta\, \mathrm{Re}h_E + \nu\cdot k\, \mathrm{Re}(h_E - h_M)\right]\frac{k_o}{m_K},$$

$$S_2 = \frac{4}{m_\mu^2}\Big[[\ell\cdot\nu - \ell^2\sin^2\theta](|h_E|^2 + |h_M|^2) + \ell_o\left(\frac{\ell\cdot k}{\ell_o k_o} - \frac{\nu\cdot k}{\nu_o k_o}\right)\nu_o \times [2|h_E|\,|h_M|\cos(\varphi_1-\varphi_2)]\Big]\frac{k_o^2}{m_K^2},$$

$$\frac{dL}{d\Omega} = \frac{1}{2\pi}\frac{\ell^2 k_o}{\ell(m_K - k_o) + \ell_o k_o \cos\theta}$$

$\ell$ is the magnitude of the muon 3-momentum; $\ell_\mu$ and $\nu_\mu$ are muon and neutrino 4-momentum; $W_{K\ell}$ is the rate for $K^+ \to \mu^+ + \nu$; $k_{max} = (m_K^2 - m_\mu^2)/2m_K$; $\theta$ is the angle between muon and gamma; $\varphi_1$ and $\varphi_2$ are the phases of $h_E$ and $h_M$. If time reversal invariance is valid, $\varphi_1 - \varphi_2 = 0$ or $\pi$ and $\mathrm{Im}h_M$ and $\mathrm{Im}h_E$ equal zero. $S_0$ represents the inner bremsstrahlung contribution (the inner bremsstrahlung photon spectrum is shown in Fig. 1), while $S_1$ and $S_2$ are the interference and direct contributions.

In the K*-pole model, Gervais et al.[4] introduced T-violation through the $KK^*\gamma$ vertex. Assuming maximum C violation by letting $\mathrm{Im}\, f_{KK^*\gamma} = \mathrm{Re}\, f_{KK^*\gamma}$ (from Eq. (I-4) we see that this implies $\mathrm{Re}\, h_M = \mathrm{Im}\, h_M = \sqrt{2}$), they found the maximum transverse muon polarization to be 57%. Since the transverse muon polarization

$$\vec{\sigma}_\mu \cdot \frac{\vec{\ell}\times\vec{k}}{|\vec{\ell}\times\vec{k}|}$$

is odd under time reversal operation, an observation of $\sigma$ component perpendicular to the $\mu$-$\gamma$ plane in the decay $K^+ \to \mu^+ + \nu + \gamma$ should be a good test of T-invariance in electromagnetic interaction. The practicality of such an experiment, however, depends heavily on the magnitude of $h_M$. If it is smaller than predicted, the transverse polarization decreases.

It was suggested[6] that weak interactions are mediated by the exchange of a vector boson-W meson. The absence of the decay mode $K^+ \to W^+ + \gamma$ which should be very abundant if it were not forbidden by kinematic reason, implies that $M_W > m_K$. The effects of a W-meson with mass larger than $m_K$ usually are very small. The inverse neutrino

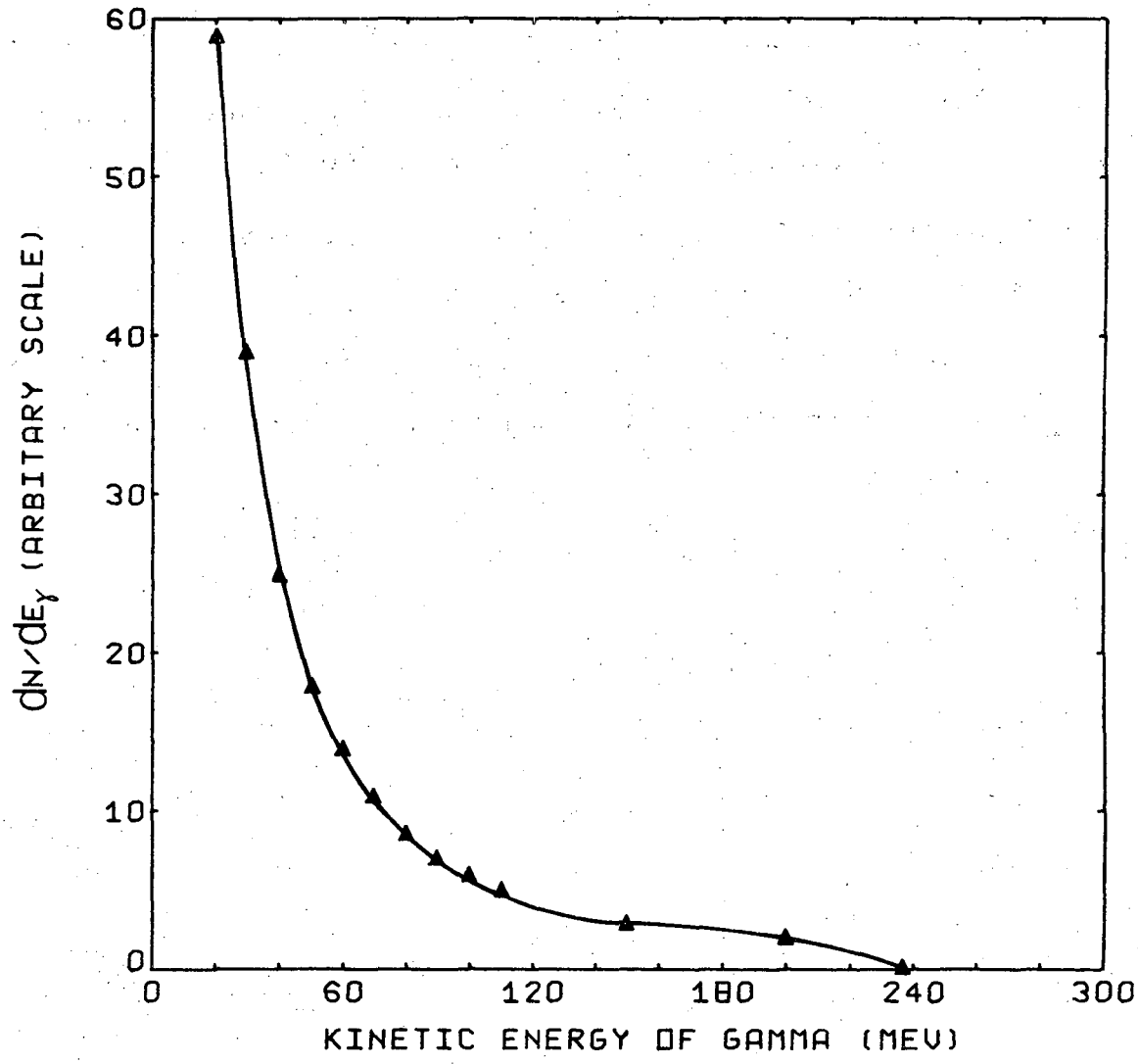


XBL 6812-6410

Fig. 1. Energy distribution of the gamma ray in $K^+ \rightarrow \mu^+ + \nu + \gamma$ for pure inner bremsstrahlung.

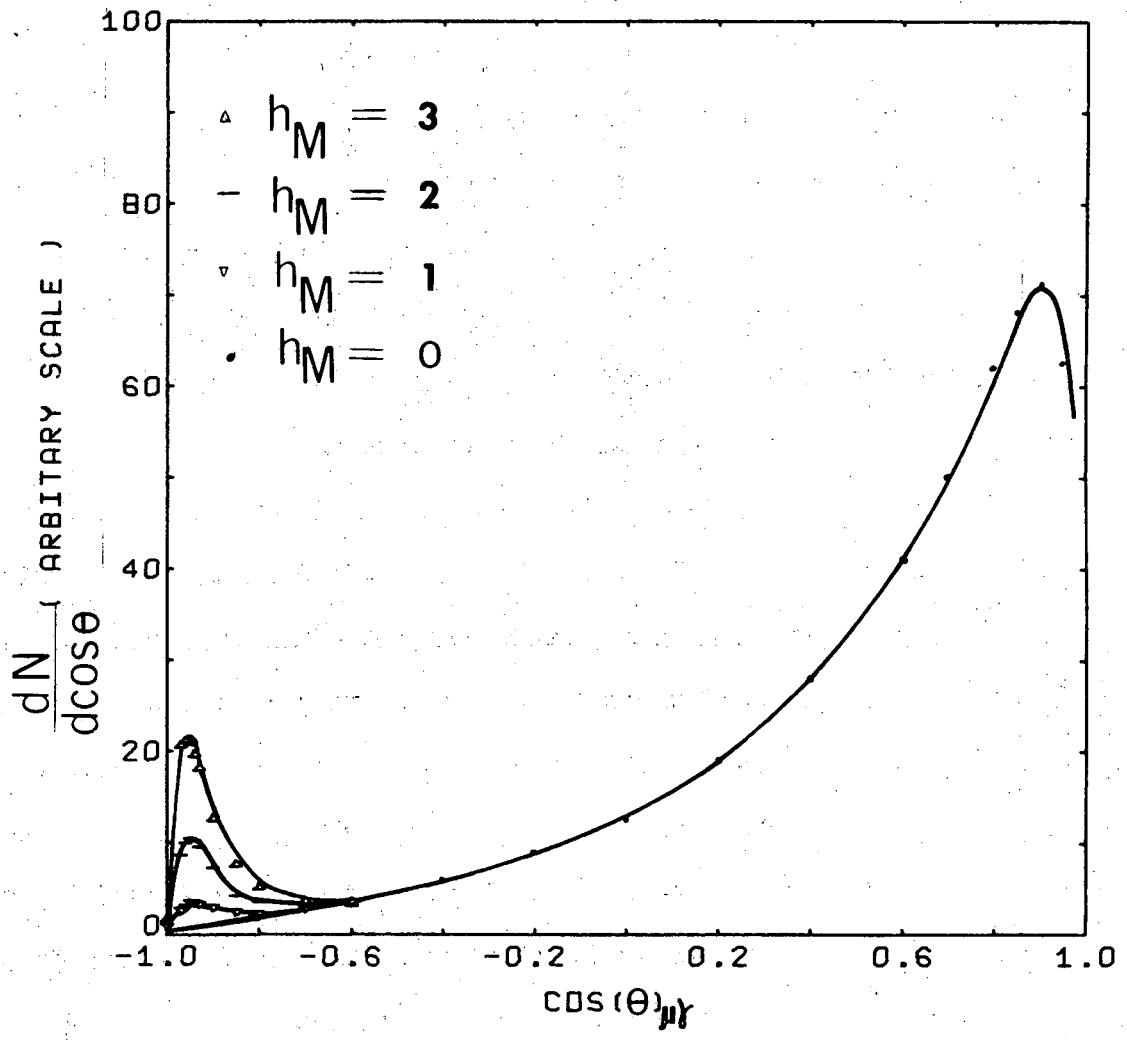


XBL 6812-6405

Fig. 2. Distribution in cos $\theta$ of the decay mode $K^+ \rightarrow \mu^+ + \nu + \gamma$ for $E_\mu$ = 139 MeV. $\theta$ is the angle between the muon direction and the gamma ray direction in a system in which $K^+$ meson decays at rest. Several curves corresponding to different values of $h_M$, the M1 form factor are shown.

events with low energy muons. Therefore we looked for events with $E_\mu$ greater than 137 MeV only. The $e^+$ from the decay mode $K^+ \rightarrow \pi^o + e^+ + \nu$ can go farther beyond the range of a 137 MeV muon. Therefore we used lead plates and Cerenkov counter to reject $e^+$ by a factor of $10^3$. Furthermore because of the finite energy resolution of the range spark chamber, the number of events due to the decay $K_{\mu 2}$ is much higher than the number of events of the decay $K_{\mu\nu\gamma}$ when the kinetic energy of the muon is greater than 142 MeV. This sets an upper limit on the muon energy for which we can possibly look for the decay $K^+ \rightarrow \mu^+ + \nu + \gamma$.

## C. APPARATUS

### a. Beam

The $K^+$ beam transport layout on the Bevatron floor is shown in Fig. 3. The total length of the beam from the target to the final focus was about 14 m. The beam had a solid angle of 6 millisteradians for a target of size 0.95 cm wide, 0.32 cm high at the second focus of the external proton beam of the Bevatron. The image size at the final focus was about 1.3 cm × 1.3 cm.

The beam was designed to meet the following requirements:

(1) This beam system reduced the number of $\pi^+$ to the same order as $K^+$ at the stopper although the production rate of $\pi^+$ from the target in the external proton beam was two order of magnitude higher than that of $K^+$.

(2) The momentum of the beam was chosen so that $\pi^+$ and $K^+$ could be easily separated and the loss of the $K^+$ mesons due to scattering and nuclear interaction through the degrader is tolerable.

(3) Since $K^+$ has a short life time ($\tau_k \sim 12$ns) the total beam length must be as short as compatible with (1) and (2). The optimum $K^+$ momentum was found to be 500 MeV/c.

(4) In order to maximize the number of $K^+$ stopped in a reasonable size of stopper, the momentum dispersion of the coming $K^+$ must be less than a few per cent of the central momentum.

The secondary beam was produced in a target at an angle of $24^o$ to the 5.3 BeV external beam of the Bevatron. It passed through the following elements:

(1) Quadrupole I which was put as close to the target as physically

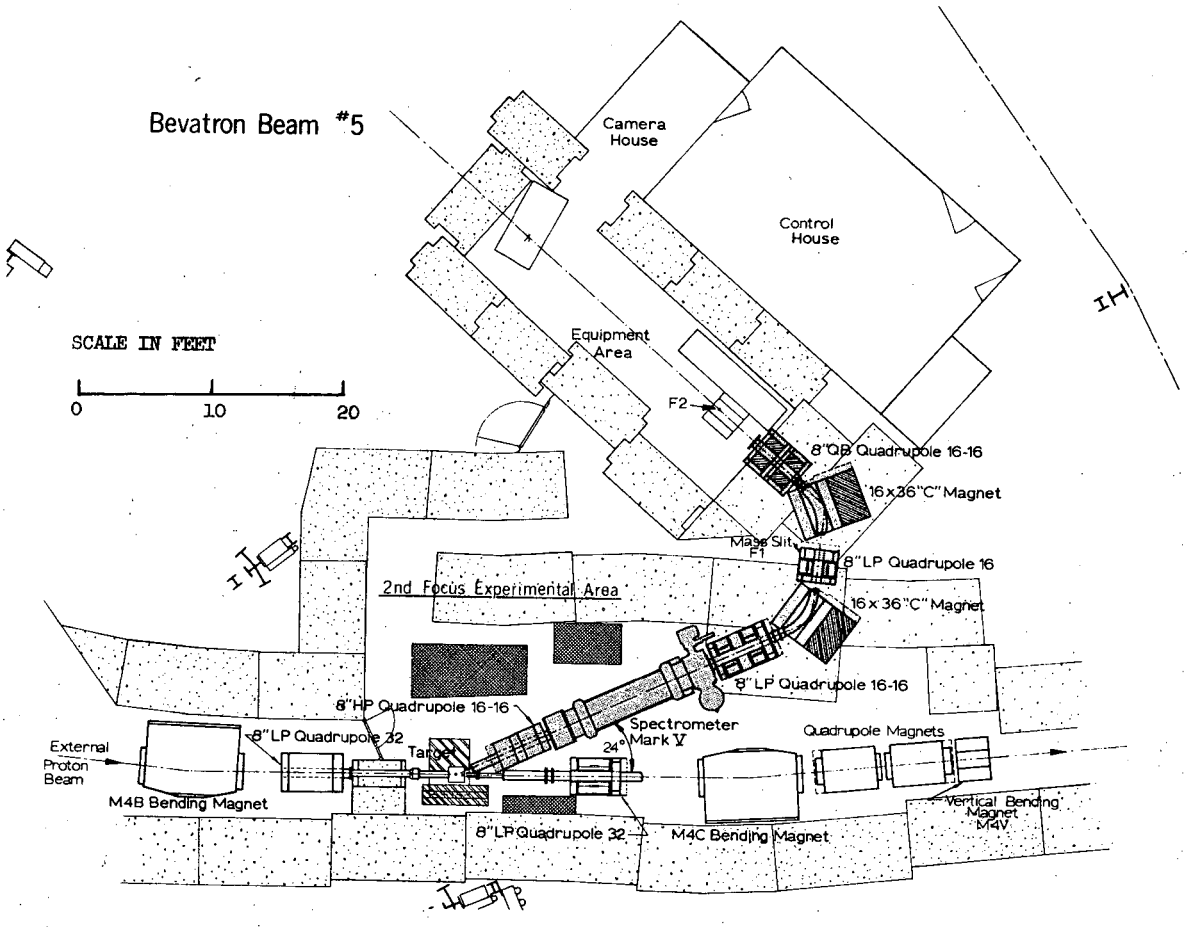


XBL 686-944

Fig. 3. Layout of the 500 MeV/c separated $K^+$ beam.

permissable to gain a large solid angle.

(2) An electrostatic separator which deflected particles vertically by distances inversely proportional to their velocities. The electrostatic separator, together with a vertical collimator at the first focus, separated $\pi^+$ from $K^+$ by a factor of 50:1.

(3) Quadrupole II which focused the beam to the first focus horizontally.

(4) Magnet I which analyzed the beam momentum and allowed a momentum spread of ±2% about the central beam momentum of 500 MeV/c .

(5) A singlet quadrupole sitting at the first focus. It serves as a field lens.

(6) Magnet II which compensated the dispersion effect of the first magnet. This function is called momentum recombination.

(7) Quadrupole IV which brought the beam to a second focus.

With $5\times10^{11}$ protons per Bevatron pulse focused on a 1-1/2 inch thick uranium target, there were $3\times10^{5}$ positive charged particles of momentum around 500 MeV/c flying down the magnet system. Most of the particles were $\pi^+$. The $K^+$ meson intensity was about 4000 per pulse at the final focus ahead of the degrader. One quarter of the $K^+$ were brought to rest by a series of counters and carbon degraders. The remainder were lost due to interactions with the carbon nucleus and multiple scattering. The $K^+$ stopper was a box of size 7.6 cm × 5.4cm×6.9cm filled with powdered carbon of low density 0.85 $gm/cm^3$. The walls of the box were made of plastic scintillator. The data were taken with the Bevatron operating under long spill (900 millisecond) conditions at a kinetic energy of 5.3 BeV. The average trigger rate of the spark chamber system was one per 2000 $K^+$ mesons stopped or one per two pulses.

b. Counters and Spark Chamber System

The counters forming the $K^+$ telescope are shown in Fig. 4. The function of this telescope was to select $K^+$ from a $\pi^+$ background and to insure that the $K^+$ stopped inside the stopper before it decayed. The $K^+$ telescope was located between the exit aperture of the last quadrupole doublet and the second focus of the beam which was 91 cm from the doublet. It consisted of five scintillation counters $S_1$, S2, S3, S4, and $\bar{S}_5$, and one threshold water Cerenkov counter $\bar{C}_k$ between S1 and S2. The Cerenkov counter detected charged particles of $\beta = v/c > 0.75$. Since 500 MeV/c $\pi^+$ have $\beta=0.963$ while the $\beta$ of the $K^+$ at the same momentum is only $\beta=0.7$ this Cerenkov counter served as an anticounter to reject $\pi^+$, $\mu^+$, and $e^+$. The counter $\overline{S}_5$ had the shape of a hollow box. Four of the six sides of the box were made of scintillators while the side facing the incoming $K^+$ and the side toward the decay-particle telescope were open.

The kinetic energy of the $K^+$ meson was considerably lower than that of the pion or lighter particles before entering the stopper. The ionization energy loss of a charged particle is approximately inversely proportional to its kinetic energy,

$$\frac{dE}{dx} \propto \frac{1}{mv^2} \ln \frac{mv^2}{ZI(1-\beta^2)^{1/2}}$$

Therefore the signals from counters S2 and S3 were bigger when the incident particle was a $K^+$ rather than a lighter particle. We set a lower limit for an acceptance on the signals from S2 and S3 to reject faster particles.

The criterion for a stopped $K^+$ was the coincidence of pulses from

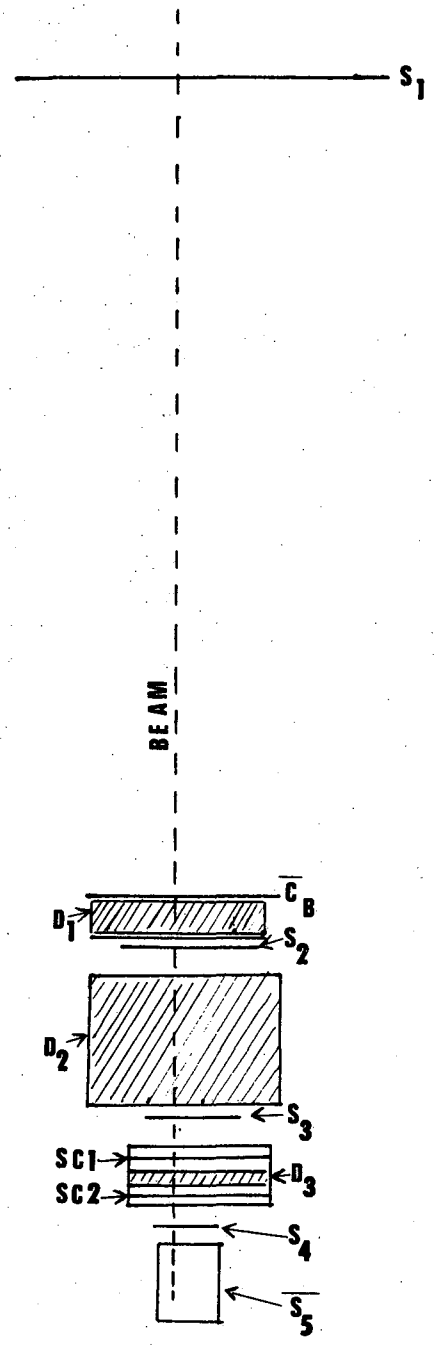


XBL 6812-6348

Fig. 4. $K^+$ telescope layout. $S_1$, $S_2$, $S_3$, $S_4$, $\bar{S}_5$ are scintillation counters; $\bar{C}_B$ is water Cerenkov counter; $D_1$, $D_2$, $D_3$ are carbon degraders; and SC1 and SC2 are spark chambers.

the scintillation counters in the $K^+$ telescope

$$K^{stop} = S1 \cdot S2 \cdot S3 \cdot S4 \cdot \bar{C}_k \cdot \bar{S}_5$$

The anticounter $\bar{S}_5$ vetoed any event upon detecting a charged particle in coincidence with S3.

The counters forming the decay-particle telescope were called T2, T3, T4, $\bar{C}_e$, and $\bar{T}_5$. The telescope was used to identify charged particles from $K^+$ decay. The water Cerenkov counter, $\bar{C}_e$, was used as a veto device against products of gamma ray conversion and the $e^+$ from $K^+ \rightarrow \pi^o + e^+ + \nu$, which were much more abundant than the muons from the decay $K^+ \rightarrow \mu^+ + \nu + \gamma$. The anticounter $\bar{T}_5$ rejected high energy particles, mainly $\mu^+$ from the decay $K^+ \rightarrow \mu^+ + \nu$. About 95% of the muons from $K^+ \rightarrow \mu^+ + \nu$ passed through $\bar{T}_5$ and thus were rejected. Approximately 15% of the muons with insufficient energy to go beyond the $T_5$ anticoincidence counter were detected in the Cerenkov anticoincidence counter. The degrader shown in Fig. 5 was variable and could be adjusted to make the range interval between T4 and $T_5$ correspond to an initial muon kinetic energy from 45 to 160 MeV.

The spark chamber trigger requirement was a T2-T3-T4-$\bar{C}_e$-$\bar{T}_5$ fast coincidence occurring in the interval from 6-35 nanoseconds after a K-stop signal, the time of which was determined by the S3 counter. The minimum allowed time between a K-stop and K-decay was chosen to insure a rejection of better than 250:1 against $K^+$ decays in flight and other prompt events, such as the scattering of the $K^+$ against the carbon stopper. The logic corresponding to a delayed $K^+$ decay was,

$$K(\text{delayed decay}) = (S1\text{-}S2\text{-}S3\text{-}S4\text{-}\bar{C}_B\text{-}\bar{S}_5) - (T2\text{-}T3\text{-}T4\text{-}\bar{C}_e\text{-}\bar{T}_5)_{\text{delayed}}. \qquad \text{(I-6)}$$

TABLE I

| Counters | Size | Photo Tube(s) | Purpose |
|---|---|---|---|
| S1 | 30cm×30cm×0.95cm | RCA6810A | S1 detected charged particles from the beam magnet system. If charged particles were detected by S1 within 600 ns before (or within 200 ns after) a K meson stopped, the event was discarded. |
| S2 | 10cm×10cm.0.95cm | RCA2067 | S2-S3-S4 defined the K meson telescope. The signals from S2 and S3 were attenuated to reject fast particles. |
| S3 | 7.6cm×7.6cm×0.6cm | RCA2067 | S3 determined the time of the $K^+$ meson entering the stopper. |
| S4 | 5.1cm×5.1cm×0.16cm | RCA2067 | Whenever S4 was triggered the particle entered the stopper. |
| $\overline{S5}$ | 7.6cm×5.4cm×6.9cm | RCA2067 | $\overline{S5}$ vetoed any prompt events. It also recorded the event when any charged particle entered the gamma spark chamber from the stopper. |
| T2 | 7.6cm×7.6cm×0.16cm | RCA2067 | T2-T3-T4 defined the muon telescope. We know the decay particle came from inside the stopper if T2 was triggered. T2 set the delayed $K^+$ decay time. |
| T3 | 25.4cm×25.4cm×1.3cm | RCA7265 | T3 insured that the particles went through $\bar{C}_e$. |
| T4 | 32cm×32cm×0.16cm | RCA8575<br>RCA8575 | We know the emitted particle entered into the range spark chambers if T4 was triggered. |
| $\overline{T5}$ | 81cm×81cm×0.95cm | 4xRCA 6810A | $\overline{T5}$ vetoed any charged particle passing through the range chamber in coincidence with T2-T3-T4. |

TABLE I (continued)

| Counters | Size | Photo Tube(s) | Purpose |
|---|---|---|---|
| $\bar{C}_k$ | 17cm×17cm×5.1cm (water filled) | RCA C31000 | $\bar{C}_k$ rejected $\pi^+$ and other lighter charged particles. |
| $\bar{C}_e$ | 27.5cm×27.5cm×1.6cm (water filled) | 4xRCA 8575 | $\bar{C}_e$ rejected $e^+$ by a factor of more than 40. |

The gamma rays were detected in three 36-module spark chambers surrounding the kaon stopper as shown in Fig. 5. In Fig. 5 all the spark chambers on the right side were 76×76 $cm^2$ , whereas the upper and the lower chambers were 30 cm × 76 cm. The plates in these modules consisted of a sandwich of a 0.8 mm thick lead between two 0.3 mm thick aluminum plates. The two modules closest to the kaon stopper were made of thin aluminum plates in order to identify charged particles entering the chamber from outside. There were no counters associated with the gamma ray chambers.

The direction of the incoming $K^+$ was measured with two 2-gap aluminum spark chamber modules placed between counters S3 and S4 in the beam telescope. The initial direction of the charged particle from the $K^+$ decay was measured with three 4-gap spark chambers labeled as SC1, SC2, and SC3 in Fig. 5. The spark chamber trigger criterion required the $\mu^+$ from $K^+$ decay to stop between counter $T^4$ and $\bar{T}_5$. There were three more sets of spark chambers associated with the $\mu^+$ telescope:

(a) Four gaps of thin aluminum sheets between $T^4$ and the degrader. They showed the direction of the charged particle after it scattered through the degrader.

(b) Twenty-eight gaps of a total thickness 9.9 grams/$cm^2$ of aluminum sheets between $T^4$ and $\bar{T}_5$.

(c) Four gaps of thin aluminum sheets after $\bar{T}_5$ to show any charged particles going beyond $\bar{T}_5$ which for some reason was not vetoed by $\bar{T}_5$ (such as an electron from muon decay).

All of the spark chambers were fired within 390 ns of a delayed

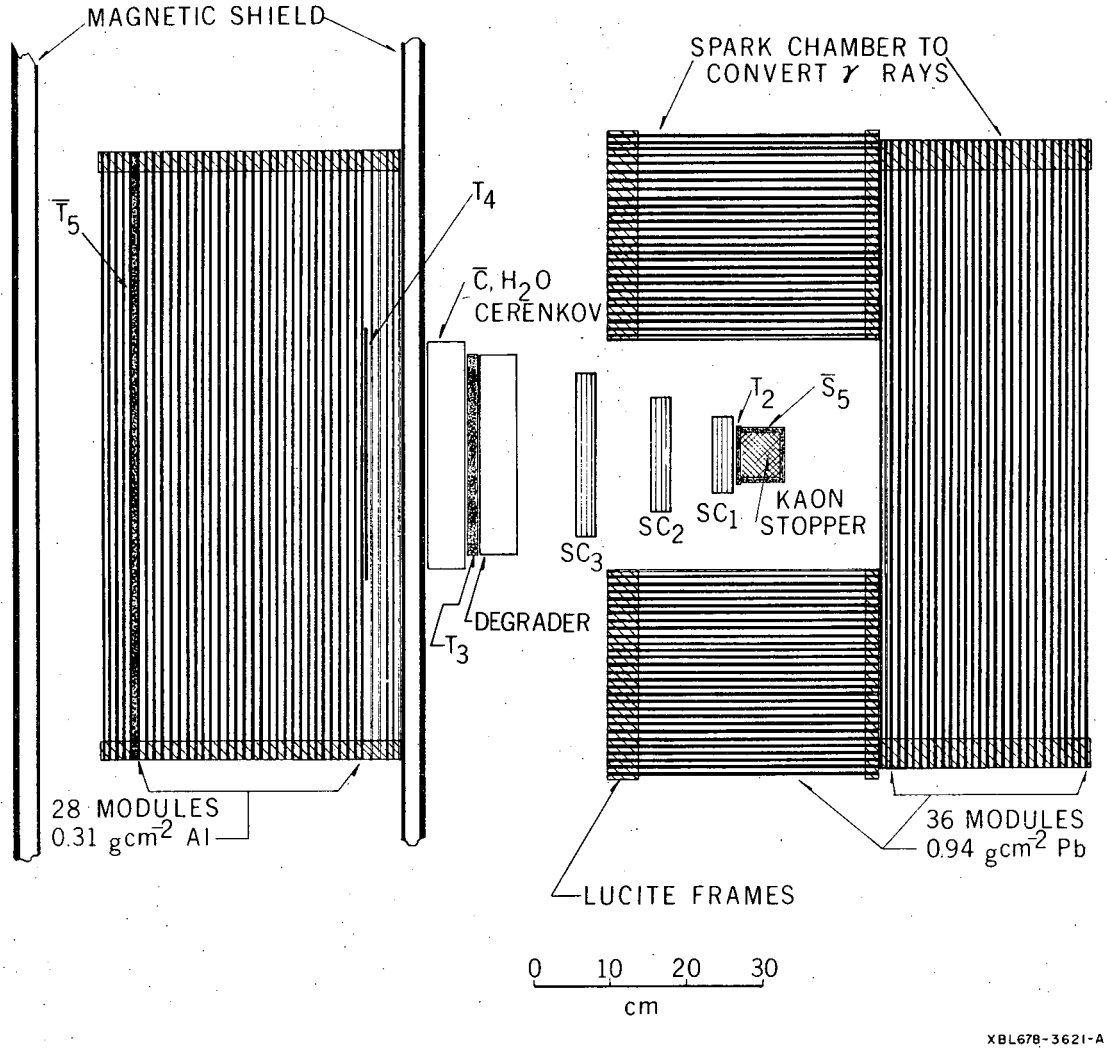


Fig. 5. Vertical cross-section of the apparatus.

$K^+$ decay signal.

Muons and electrons can generally be distinguished by the nature of their tracks in the aluminum spark chambers. The track of a muon was straight and continuous while that of an electron was usually broken and scattered. The range of the muon was determined by measuring its depth of penetration into the 28 module aluminum plate spark chambers between $T_4$ and $\bar{T}_5$. The degrader ahead of $T_3$ was variable. For $K^+ \rightarrow \mu^+ + \nu + \gamma$ decay mode we used three pieces of degraders,

(1) 29.6 gm/cm$^2$ or 2.5 radiation lengths of copper before $T_3$ (radiation length of copper = 12 gm/cm$^2$),

(2) 7.8 gm/cm$^2$ or 1.2 radiation lengths of lead ahead of spark chambers SC3, and

(3) 11.8 gm/cm$^2$ or 1.8 radiation lengths of lead ahead of spark chambers SC2 (radiation length of lead = 6.52 gm/cm$^2$).

For $K^+ \rightarrow \mu^+ + \nu$ decay we changed the thickness of the copper sheet to 35.7 gm/cm$^2$ of copper. This was the only difference between the two runs.

The lead sheets were used to attenuate the positrons from the decay mode $K^+ \rightarrow e^+ + \pi^o + \nu$.

The spark chambers were sensitive for a period of 390 ns after the $K^+$ decay took place. The minimum delay between two triggers was chosen to be 250 milliseconds to allow the apparatus to recover. The clearing fields which cleared away the remaining ions due to previous charged particles in the spark chambers, were 50 volts for the range chambers, 40 volts for the gamma ray conversion chambers and 30 volts for the beam chambers. A total of 18 views of the 9 sets of spark chambers

were photographed by a camera 10 m away. We used 24 mm × 36 mm frames of Tri-x film. The f-number of the lens was 8. We observed 566,858 delayed $K^+$ decays, among which 26,807 short range $\mu^+$, which did not pass through $\bar{T}_5$ nor triggered $\bar{C}_e$, were able to pass the trigger criterion (I-6). Whenever a particle satisfied the trigger ciriterion, the chambers fired and we took a picture of the event.

The electronic logic system is shown in Fig. 6 and Fig. 7.

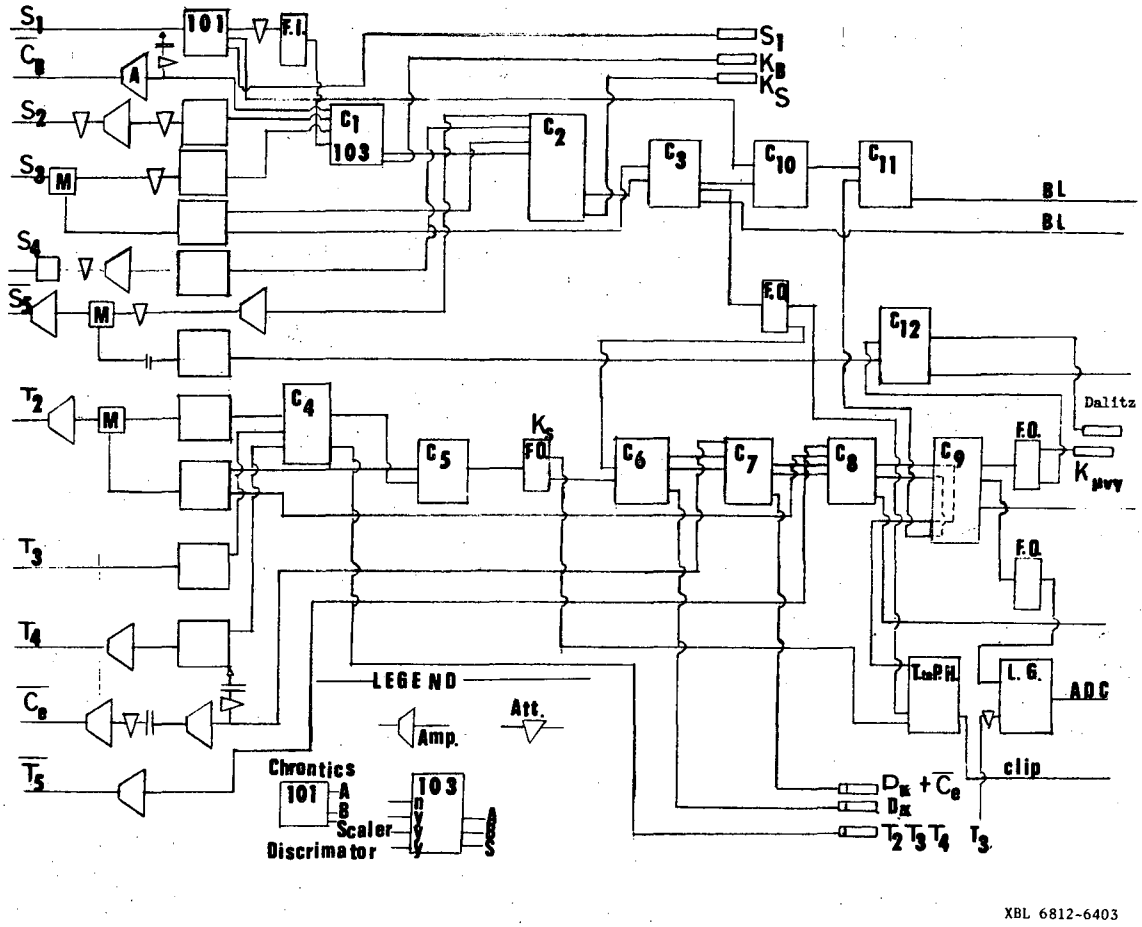


Fig. 6. Schematic diagram I of the electronic fast logic for the experiments.

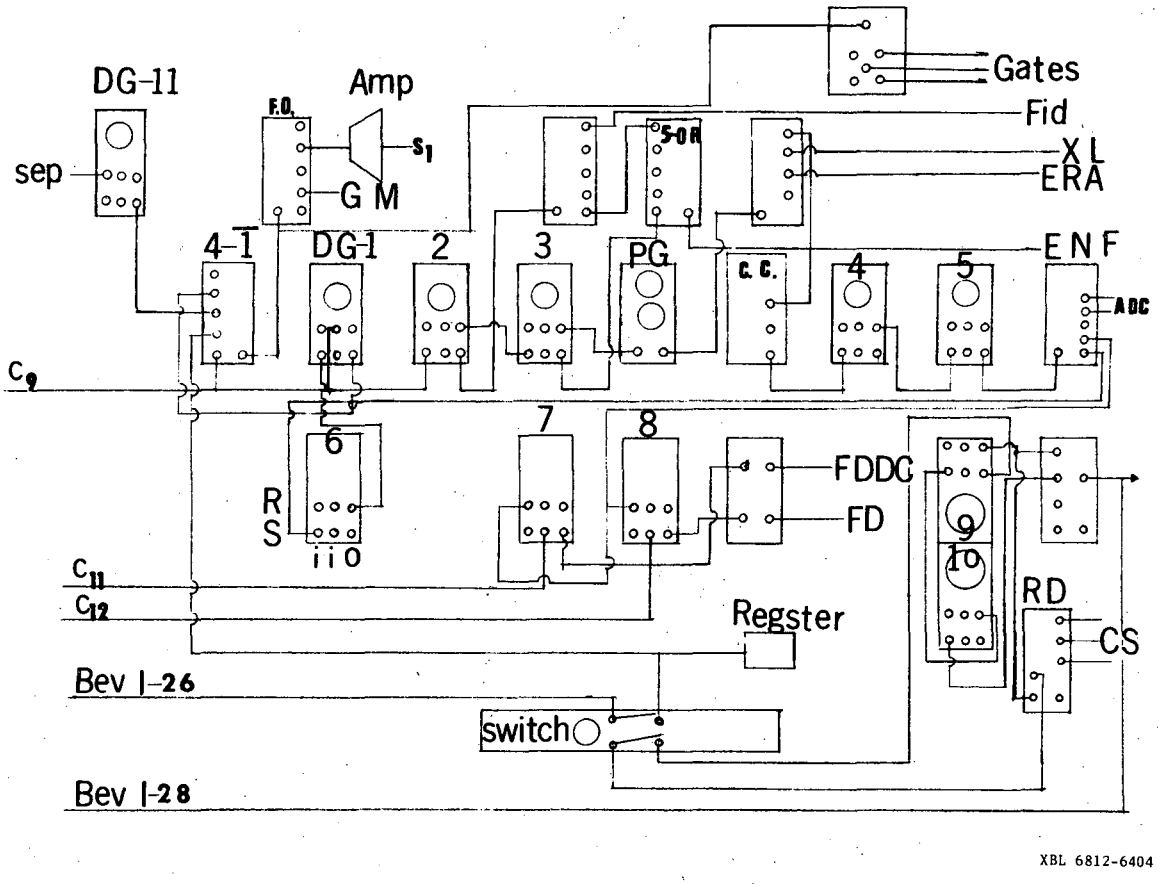


Fig. 7. Schematic diagram II of the electronic fast logic for the experiments.

LEGEND

A D C : Analog to Digital Converter

Amp : Amplifier

B L : Binary Lights

C. C. : Camera Control

C S : Camera Shutter

D G : Delayed Gate

E N F : Event Number Flash

E R A : Event Register Advance

F D : Fixed Data

F D D C : Fixed Data Display Control

Fid : Fiducials

F O : Fan Out

F I : Fan In

Gates : Gates for Chronetics

G M : Gate Monitor (scope)

L. G. : Linear Gate

L S : Level Shift

P G : Pulse Generator

R : Reset

R D : Relay Driver

S : Set

Sep : Separator Interlock

T. to P. H. : Time to Pulse Height Conversion

X L : Xenon Lamp

## D. DATA REDUCTION AND ANALYSIS

The purpose of data reduction was to select events with appropriate muon energies and converted gamma rays. The 26807 pictures taken during 164 hours of running at the Bevatron were scanned with SPASS, the automatic computer-scanning system developed by Deutsch at MIT.[8] All views of the chambers were scanned by this system except the 6 views of the gamma-ray conversion chambers which were scanned manually. Using the information from the SPASS scanning we reconstructed the track of the incoming $K^+$ and the track of the charged decay particle, $\mu^+$. If there were two or more tracks in either of the $K^+$ tracking chambers or the $\mu^+$ tracking chambers the event was discarded. If either the $K^+$ track or the $\mu^+$ track was missing, the event was also discarded. Because of the above criteria, 16.4% of the total pictures were discarded.

The position of the $K^+$ stop was inferred from the intersection point of the track of the $K^+$ and the track of the $\mu^+$. Ideally this should be a point. However since the $K^+$ was scattered before it actually stopped, the position of the $K^+$ stop was then defined to be the point on the $\mu^+$ line with the minimum distance between this point and the $K^+$ line. We discarded all events with this minimum distance larger than 1 cm or with the intersection point outside of the stopper. Five percent of the events were thrown away because of this criterion.

The muon range chambers were also scanned by SPASS. From this information we obtained the portion of the muon track after the muon scattered through the degrader. Sometimes when we combined this part of the data with that obtained from the tracking chambers, the picture numbers used in the two scannings did not match. For this reason, 4.3%

of the events were discarded. This loss was due to a defect in the automatic scanning device.

The muon stop position inside the muon range chamber was measured by SPASS in both the top and side views. Occasionally SPASS missed the last few sparks in one view or the other, before the muon stopped or SPASS added some nearby random sparks to the muon track in either of the two views. Also 17% of the muon stopped in the range chambers decayed into electrons before the chambers were fired. When the emitted electron made an angle less than 30 degrees with respect to the muon direction in one view, SPASS could not tell the muon track from the electron track in that view. Therefore the gap numbers in the two views were different in these cases. In order to get a good energy resolution, we required the difference between the number of gap penetrated by the muon deduced from the top view and that from the side view be less than 3 gaps or 1.6 MeV muon kinetic energy. As a result 4% of the remaining pictures were discarded because of inconsistency of the gap numbers in the two views.

We have set the following criteria for the smoothness of the muon track to improve the precision of the calculation of the muon energy and to reject scattered electrons

(a) The scattered angle through the three tracking chambers of muon was less than $11^{\circ}$.

(b) The scattered angle through the copper degrader, and T3. T4 was less than $23^{\circ}$,

From the track inferred from the tracking chambers we could predict the initial position of the muon track in the range chamber

if the muon had not been scattered. The distance between the predicted position and the actually measured position, S, also gave some information of scattering. Therefore we required

(c) S be less than 5 cm,

(d) The angle between the initial direction of the track determined by the first 4 sparks in the muon range chamber and the mean direction of the track in the range chamber be less than $22.5^{\circ}$. Inside the range chambers the multiple scattering angles of the electrons are considerably larger than those of the muons. Therefore this criterion also helped discard $K_{e3}$ background events.

Thirty percent of the remaining pictures were discarded because of the above criteria. The muon energies of those pictures left should be well represented by their total ionization energy loss through various materials. The calculation was confirmed by the $K\mu_2$ data as shown below.

We used the muons from the decay mode $K\mu_2$ as a calibration of the determination of the muon kinetic energy from the range. The calculated mean energy was lower by 1.5 MeV than the known muon energy of 152.5 MeV for $K^+ \rightarrow \mu^+ + \nu$. The calculated energy values were then multiplied by a correction factor 1.01. The only change in our setup for $K^+\mu_2$ and $K^+ \rightarrow \mu^+\nu\gamma$ is one piece of copper degrader of a thickness of 5.9 gm. After making the above correction, we believe the error of the calculated mean muon energy for muons from $K^+_{\mu\nu\gamma}$ decay mode is much smaller than the energy uncertainty due to straggling which is 4 MeV for 150 MeV muons.

The detection efficiency of the muon telescope was deduced from

the range curves shown in Fig. 8, which showed the solid angle of the muon telescope was maximum for 138 MeV of muon energy. The threshold Cerenkov counter rejected about 15% of the muons at that energy.

We selected the events with calculated muon kinetic energy between 137 MeV and 142 MeV. There were 610 $K^+_{\mu\nu\gamma}$ candidates left. Assuming inner bremsstrahlung only, we expected 228 events. The ratio of $K_{\mu 2}$ events to $K_{\mu\gamma\nu}$ events was about 2 to 1 in the above energy interval. The identification of a gamma ray shower is crucial to separate $K_{\mu\gamma\nu}$ events from $K_{\mu 2}$ background events.

The gamma-ray chamber views of these pictures were scanned manually on a Recordak machine. Gamma rays were identified by the showers in the lead spark chambers. The criteria for a gamma ray shower were:

(a) There was a cluster of three or more sparks in successive plates in the lead spark chambers. The main part of the cluster should be within roughly 1 cm of the averaged shower direction, and

(b) There were no sparks as part of the cluster in the first two plates closest to the $K^+$ stopper. With this requirement most of the charged particles coming into the gamma ray chamber were thrown away, and

(c) If the track of a gamma ray shower was straight, the plate farthest from the $K^+$ stopper should not be fired so that charged particles coming from outside would not contaminate the real events. However if we could identify the track as a shower, we would not require the last gap to be empty, and

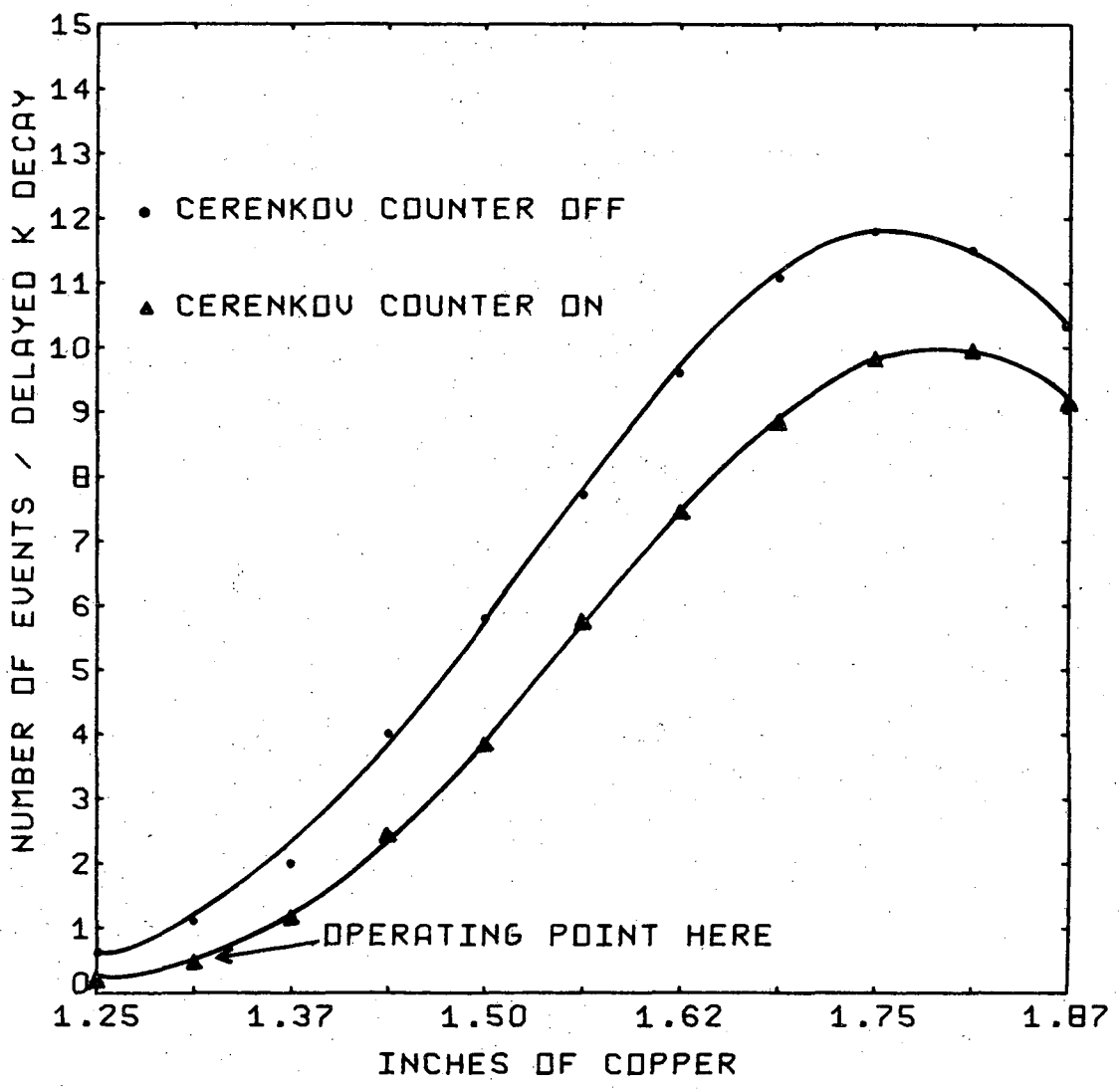


XBL 6812-6411

Fig. 8. Range curve in inches of copper of charged particles from $K^+$ decay. The peak shown is due to $K_{\mu 2}$. The operation piont where the data of $K^+ \rightarrow \mu^+ + \nu + \gamma$ was taken is also shown.

(d) The angle, $\varphi$, between the line defined by the $K^+$ stop point and the first spark (closest to the $K^+$ stopper) of the spark cluster and the line defined by the first spark and the average position of the next two sparks of the cluster, was less than $40^\circ$.

The criterion (d) was necessary to discard all events with gamma ray showers or recoiled protons from sources other than those in the $K^+$ stopper. Six such events with the above angle from $45^\circ$ to $100^\circ$ were discarded. In order to justify this cut-off, we scanned some pictures with gamma ray showers from the decay $K^+ \rightarrow \pi^+ + \pi^\circ$. When both gamma rays were converted, we calculated their energies from kinematic conditions. The distribution curves with respect to $\varphi$ corresponding to two gamma ray energy intervals are shown in Fig. 10a and Fig. 10b. We found fewer than 5% of the events had $\varphi$ greater than $45^\circ$.

After the selection based on the above criteria there were 27 events associated with a converted gamma shower. The detection efficiency of the gamma ray as a function of $\cos\theta$ is calculated in Appendix (c) by a Monte Carlo method. The result of the calculation is shown in Fig. 11.

To estimate how many background gamma rays we had in our sample, we scanned two sets of events. The muon energy of the first set was between 144 and 146 MeV and that of the second set was between 152.5 and 153.5 MeV, where $K_{\mu 2}$ events were dominant. Each set contained about 600 pictures. They were scanned by the same criteria as (a) through (d). We found no essential difference between these two samples of data. This distribution curve of gamma rays, which are certainly all

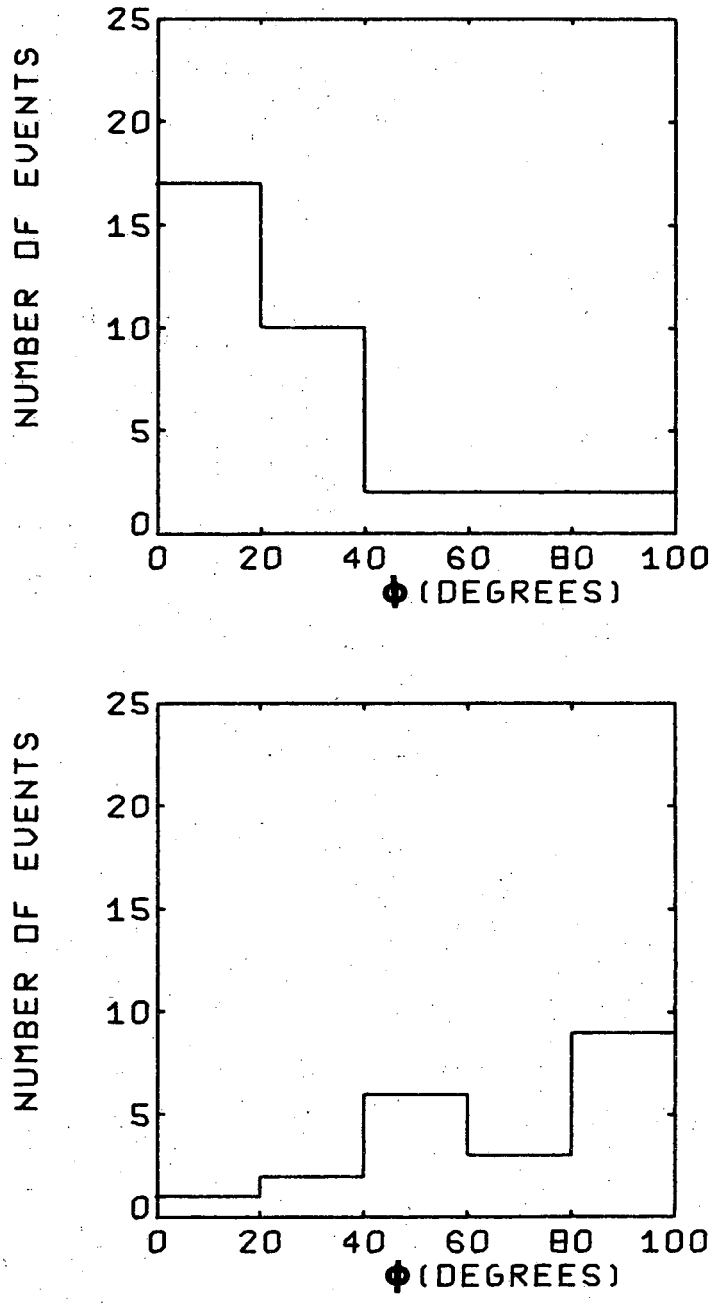


XBL 6812-6346

Fig. 9a. Distribution in the angle $\varphi$ of the sample of $K^+ \rightarrow \mu^+ + \nu + \gamma$. $\varphi$ is the angle between the direction of the flight of the gamma ray (as determined by the $K^+$-stop position and the conversion point) and the average direction of the shower in the lead plate spark chambers.

Fig. 9b. Distibution in the angle $\varphi$ of the sample of $K^+ \rightarrow \mu^+ + \nu$ + chance track in shower chambers. The peak at $0^o$ is missing as the chance tracks are unrelated to the $K^+$ decay.

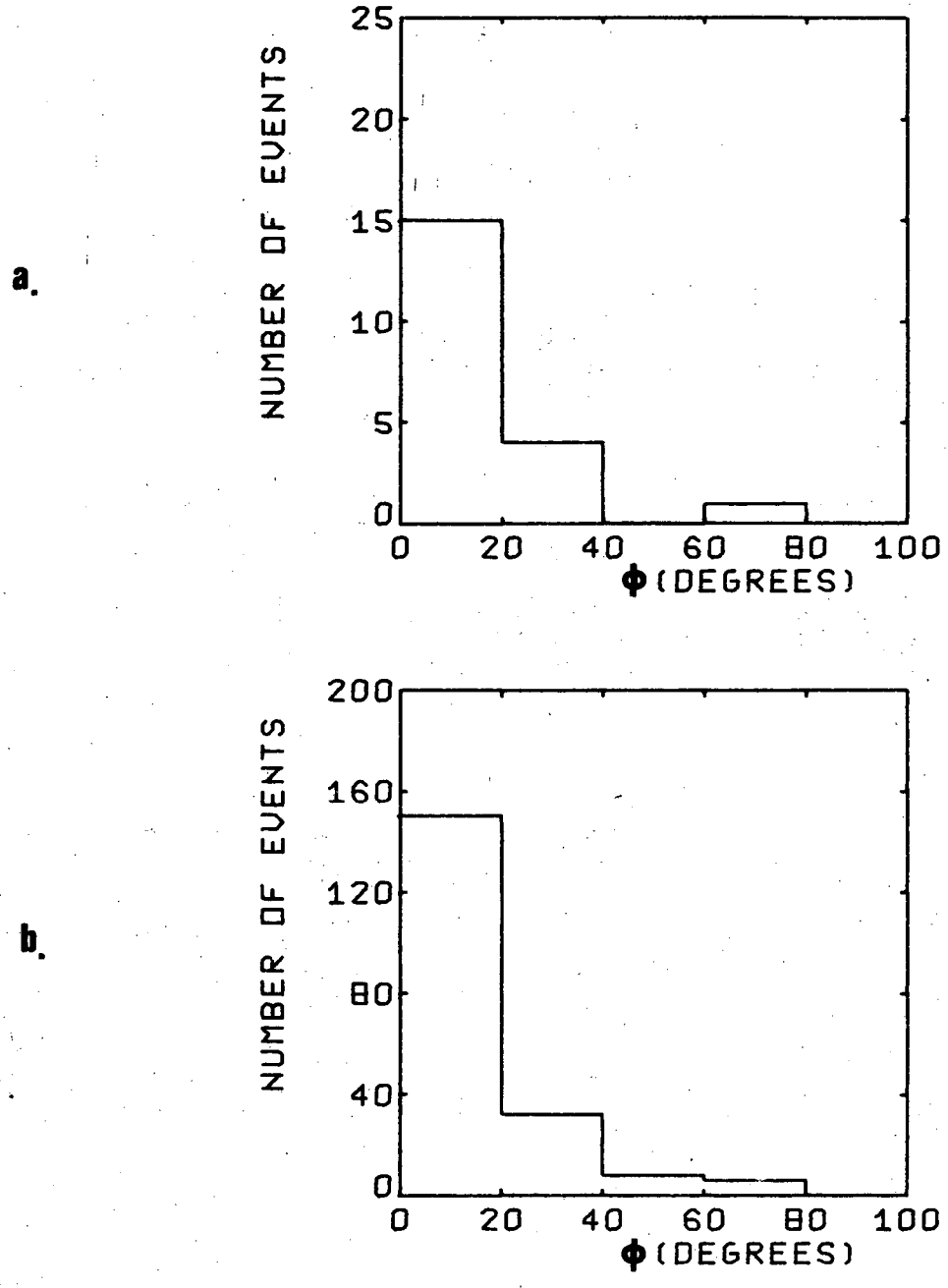


XBL 6812-6347

Fig. 10. Distribution in the angle φ with

(b) $E_\gamma > 100$ MeV.

(a) $E_\gamma < 40$ MeV.

φ is the angle defined in Fig. 9.

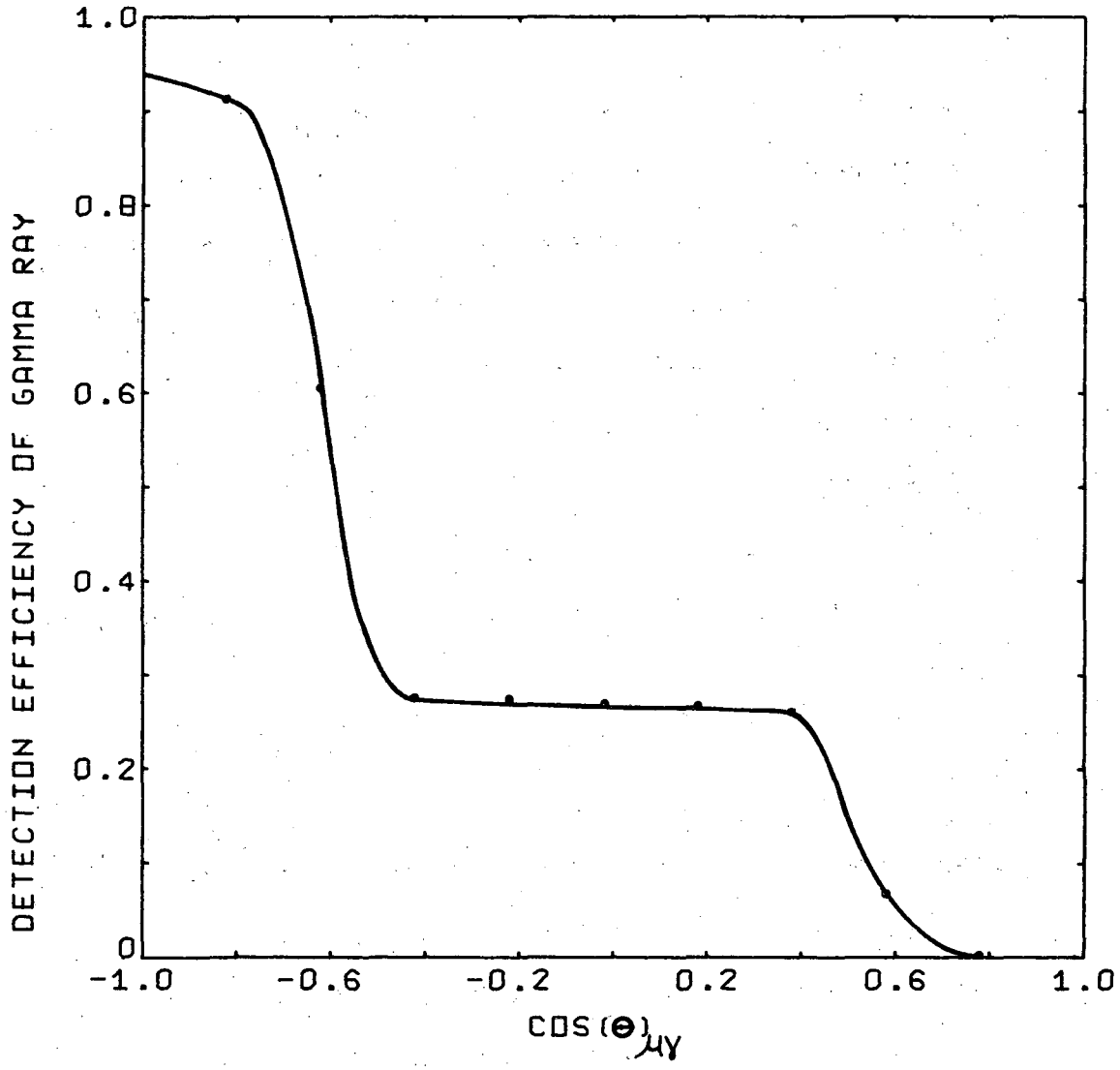


XBL 6812-6408

Fig. 11. Detection efficiency of the gamma ray from $K^+$ as a function of cos $\theta$ (the angle between the muon and the gamma direction) for events with the kinetic energy of muons between 137 and 142 MeV.

spurious in this data, with respect to the angle $\varphi$ defined above is shown in Fig. 9. Taking a cut off point at $\varphi = 40^{\circ}$ we were left with three background events from a sample twice as large as the data sample size. Therefore we conclude that there are one and one half expected background events in our data. The probability for the gamma rays of these background events to appear in the backward zone with respect to the muon direction is proportional to the solid angle and is extremely small. As a result we conclude that these background events will not simulate the direct decay events of $K^+ \rightarrow \mu^+ + \nu + \gamma$ at the level of sensitivity we have reached in this experiment.

The main background events that can simulate the direct decay of $K^+ \rightarrow \mu^+ + \nu + \gamma$ are as follows:

(1) $K^+ \rightarrow \pi^+ + \pi^0$ followed by the processes $\pi^0 \rightarrow \gamma + \gamma$ in flight and $\pi^+ \rightarrow \mu^+ + \nu$ in flight. The kinetic energy of the muon could be as high as 134 MeV if the muon was emitted in the forward direction in the center of mass system of the $\pi^+$. Since we had neither $4\pi$ solid angle nor 100% conversion probability for the gamma rays, frequently one of the two gamma rays did not convert (roughly 25% of the $K^+ \rightarrow \pi^+ + \pi^0$ events). Because the detection efficiency was larger for backward gamma rays with respect to the muons than for forward gamma rays, it was very likely that we detected only the backward gamma ray from the $\pi^0$ decay and took it as the structure dependent decay of $K^+ \rightarrow \mu^+ + \nu + \gamma$. To eliminate this kind of background we cut off any event with muon energy below 137 MeV.

The branching ratio of $K_{\pi 2}$ is 21% of the total decay rate of the $K^+$ meson. Fewer than 2% of the $\pi^+$ from the decay $K^+ \rightarrow \pi^+ + \pi^o$ could decay in flight before entering the degrader. After the pion entered the degrader it lost too much energy to emit a high energy muon to make the total range of the pion and the muon greater than the range of a 128 MeV muon and therefore could not be taken for a $K^+ \rightarrow \mu^+ + \nu + \gamma$ events with muon energy greater than 137 MeV. Only 5% of the $\pi$-decay muons from the above 2% $\pi^+$ decay in flight had kinetic energy greater than 130 MeV. A Monte Carlo calculation showed that less than 1/15 of the above muons with energies between 130 and 134 MeV could penetrate the equivalent range of a 137 MeV muon because of straggling. A $\pi^+$ from the decay $K^+ \rightarrow \pi^+ + \pi^o$ could emit a muon such that the total range of the $\mu^+$ and $\pi^+$ appeared to be greater than the range of a 137 MeV muon. From the above calculation we found the upper limit of such events was four. However, from the result of a scanning of $K_{\pi 2}$ events which were taken under the same condition as the $K^+ \rightarrow \mu^+ + \nu + \gamma$ sample except that the degrader in the muon telescope was readjusted for 108 MeV pion, we found that there were twice as many $K_{\pi 2}$ events with both gamma rays converted as those with only one gamma ray converted. Therefore we believe that there were less than one background event due to $K^+ \rightarrow \pi^+ + \pi^o$ in our sample. The fact that we did not see any events with 2 gamma showers beyond 137 MeV muon kinetic energy suggested that there were fewer than 0.5 $K^+ \rightarrow \pi^+ + \pi^o$ events.

(2) $K^+ \rightarrow \mu^+ + \pi^o + \nu$ where one of the two gammas from the $\pi^o$ decay was not converted. The highest muon energy of these events is 134 MeV. A Monte Carlo calculation was made to estimate how many $K_{\mu 3}$ events would simulate $K_{\mu\nu\gamma}$ events. We randomly generated $4\times10^6$ $K_{\mu 3}$ events according to the distribution in the Dalitz plot calculated from V-A theory and from the assumption that the effect of the terms with the form factor $F_-$ is negligible. The uncertainty in the muon energy measurement was assumed to be $\pm 4$ MeV. We found 63 events with muon range greater than that of 134 MeV muon. Furthermore, for $K_{\mu 3}$ events with muon kinetic energy greater than 125 MeV, the detection efficiency of the gamma rays is roughly the same as that of the gamma rays from the $\pi^o$ of $K_{\pi 2}$ events. As we discussed in the previous section that the probability of detecting only one gamma ray was about 25%. Taking the branching ratio of $K_{\mu 3}$ to be 3.4%, we concluded that there were fewer than 0.13 background events of $K^+ \rightarrow \pi^o + \mu^+ + \nu$ in our sample.

(3) $K^+ \rightarrow e^+ + \pi^o + \nu$, where the $\pi^o$ decays into $\gamma + \gamma$ in flight. If only one of the two gamma rays was converted, the $K_{e3}$ events could simulate the direct decay of $K^+ \rightarrow \mu^+ + \nu + \gamma$. The cut-off of low energy muons did not eliminate $K_{e3}$ background events because the electrons could go beyond the range of 137 MeV muons. Therefore it was necessary to use Cerenkov counter and lead plates to identify electrons. We used 3 radiation lengths of lead between the 3 sets of muon tracking spark chambers. Behind the tracking chamber there was a copper degrader of 2.46 radiation lengths. It was shown by Wilson[9] that after two radiation lengths of lead the probability of attenuation of a 100 MeV

electron is 0.28 while the probability of conversion of the electron into two or more electrons with energy greater than 5 MeV is 0.54. When two or more sparks appeared in any one plate of the tracking chambers, the event was discarded because the origin of the track was suspected to be an electron.

We scanned 150 pictures of 200 MeV electrons stopped in lead plate spark chambers. The data was taken by Cronin.[10] We found the probability was less than 3% for an electron to go through the lead plates corresponding to the thickness of the degraders we used without being attenuated, converted or scattered by an angle greater than $15^{\circ}$ in either view. The threshold water Cerenkov counter, $\bar{C}_e$, detected particles with $\beta > 0.75$. From the test with cosmic rays passing through $\bar{C}_e$ we knew the efficiency of $\bar{C}_e$ against high velocity particles was better than 97.5%. Less than one half of the electrons which went through the degrader would stop in the range spark chambers. The probability of an electron stopped in the range chamber to be taken as a muon of kinetic energy between 137 and 142 MeV was about 25%. The probability of detecting only one gamma ray from $\pi^{o}$ decay for the $K^{+}_{e3}$ decay mode was less than 50%. We concluded that there were fewer than 1/2 $K^{+} \rightarrow \pi^{o} + e^{+} + \nu$ background events in our sample.

(4) A charged particle, most likely to be a pion, entered the apparatus within 340 nanoseconds after a $K^{+}$ meson stopped. This could cause two kinds of background events:

(a) there was a gamma ray shower due to the $K^{+}$ meson decay but the muon track was produced by the $\pi^{+}$ which was scattered into the muon telescope.

(b) the muon track was from the real $K^+$ meson decay but the gamma ray was produced by the incoming $\pi^+$ interacting with the nucleus. For example, the reaction $\pi^+ + n \rightarrow \pi^o + p$ with only one gamma ray converted. ($\pi^o \rightarrow \gamma + \gamma$)

When we took the data we marked the picture with a lamp whenever the S1 counter detected a charged particle between 20 to 200 ns after a $K^+$ meson stopped. Since the particles from the Bevatron usually came in a spike of 100 ns width, most of the above background events were detected by S1 and thus rejected. One-seventh of the total pictures belonged to this category and were discarded.

Table II. Discards of pictures due to various criteria.

| Total Pictures Taken | $26.6 \times 10^3$ | |
|---|---|---|
| Criteria | $N_i$ (Number of pictures left) | $E_i = N_{i-1}/N_i$ efficiency |
| 1) One and only one track in the $K^+$ and the $\mu^+$ tracking spark chambers | $22.2 \times 10^3$ | 83.6% |
| 2) Pictures with the two scanning numbers matched | $21.2 \times 10^3$ | 95.7% |
| 3) Pictures with the two gap numbers matched | $20.4 \times 10^3$ | 96.4% |
| 4) Minimum distance between the $K^+$ stop position and the kaon track less than 1 cm | $19.3 \times 10^3$ | 95% |
| 5) Muon scattering criterion (a) | $18.2 \times 10^3$ | 95% |
| 6) No. of pictures with calculated muon energy between 130 and 142 MeV | 1351 | - |
| 7) Muon scattering criterion (d) | 1231 | 91% |
| 8) Muon scattering criterion (b) | 1051 | 85.2% |
| 9) Muon scattering criterion (c) | 965 | 92% |
| 10) No. of pictures with calculated muon energy between 137 and 142 MeV | 712 | - |
| 11) $\pi^+$ after $K^+$ events discarded | 610 | 84% |

Overall detection efficiency for the muon = $E_1 \cdot E_2 \cdot E_3 \cdot E_4 \cdot E_5 \cdot E_7 \cdot E_8 \cdot E_9 \cdot \bar{C}_\mu \cdot \Omega_\mu = 41\%$

where $\bar{C}_\mu$ is the percentage of events not vetoed by $\bar{C}_\mu$, $\bar{C}_\mu \sim 85\%$ and $\Omega_\mu$ is the solid angle for the muon, $\Omega_\mu(E_\mu \sim 138) = 100\%$.

## E. Results

We found 27 events with muon kinetic energy between 137 and 142 MeV with an accompanying converted gamma ray shower. The effective $K_{\mu 2}$ events was defined as the product of the total number of $K_{\mu 2}$ events observed during the $K^+ \to \mu^+ + \nu + \gamma$ runs and the overall detection efficiency (not including the gamma ray) of the $K^+ \to \mu^+ + \nu + \gamma$ events in the muon kinetic energy interval $137 < T_\mu < 142$ MeV as discussed in the data reduction. The observed 27 $K^+ \to \mu^+ + \nu + \gamma$ events corresponded to $2 \times 10^5$ effective $K_{\mu 2}$ events.

A maximum likelihood analysis was performed to calculate the form factors $h_m$, $h_E$ in Eq. (I-5) from the observed distribution of the angle, $\theta_{\mu\gamma}$, between muon and the gamma ray. The form factors were assumed to be real because with the limited number of events as we had, we did not expect to detect the effect due to T-violation. We constructed the likelihood function, depending only on $h_M$ and $h_E$, as the product over all the events of the separate probability distribution:

$$L(h_E,h_M) = \prod_{i=1}^{27} \frac{f_i(h_M,h_E,E_\mu^{(i)},\cos\theta_{\mu\gamma}^{(i)})}{S(h_E,h_M)} \qquad \text{(I-7)}$$

where $f(h_E,h_M,E_\mu,\cos\theta_{\mu\gamma})$ equals the differential decay rate defined in Eq. (I-5), $E_\mu$ is the energy of the muon and the normalization factor $S(h_M,h_E)$ has the form:

$$S(h_M,h_E) = \int_{137}^{142} \int_{-1}^{1} \cos\theta_{\mu\gamma} dE_\mu f(h_M,h_E,E_\mu,\cos\theta_{\mu\gamma}) g(E_\mu,\cos\theta_{\mu\gamma}) \qquad \text{(I-8)}$$

where $g(E_\mu,\cos\theta_{\mu\gamma})$ is the detection efficiency of an event with muon energy $E_\mu$ and the opening angle $\theta_{\mu\gamma}$.

Our result for $h_{M,E}$ is the value which maximizes the likelihood function in Eq. (I-7). The result of this analysis is shown in Fig. 12. Each closed curve shows where $L(h_M,h_E)$ has dropped to a constant fraction of the maximum $L(h_M,h_E)$. There is a 40% probability that the true values of $h_M$ and $h_E$ fall inside the first closed curve (1/e). The two vertical lines at $h_M = \pm 2$ are predicted by Gervais et al. based on $SU_6$ and K* pole model when we neglect the dependence of the form factor $h_M$ on $E_\gamma$. The line $h_E = 0.8\ h_M$ is predicted in reference 5 by using Fubini type unsubtracted dispersion relation. The two intersection points at $h_E = \pm 1.6$ and $h_M = \pm 2$ are incompatible with our result. It seems the value predicted by Gervais et al. is at least a factor of two too big. The value predicted by Jackson is consistent with our data.

Because the mass of the vector mesons are lower than those of the pseudo-vector mesons we expect that the M1 term is much larger than the E1 term. Therefore it is reasonable to assume that the E1 term is negligible. We did a maximum likelihood analysis with respect to the M1 term only. As before we have

$$L(h_M) = \prod_{i=1}^{27} \frac{1}{S(h_M)}\, f_i(h_M, E_\mu^{(i)}, \cos\theta_{\mu\gamma}^{(i)})$$

and

$$S(h_M) = \int_{137}^{142} \int_{-1}^{1} d\cos\theta_{\mu\gamma}\, dE_\mu f(h_M, E_\mu, \cos\theta_{\mu\gamma}) g(E_\mu, \cos\theta_{\mu\gamma}) \qquad \text{(I-9)}$$

The result is shown in Fig. 13. We found $h_M = 0.05 \pm 1.2$. The upper limit of the absolute value of $h_M$ at 95% confidence level (2 standard deviations from the maximum value) is 2.3. Our result is consistent with the predictions of the K*-pole model in the case that

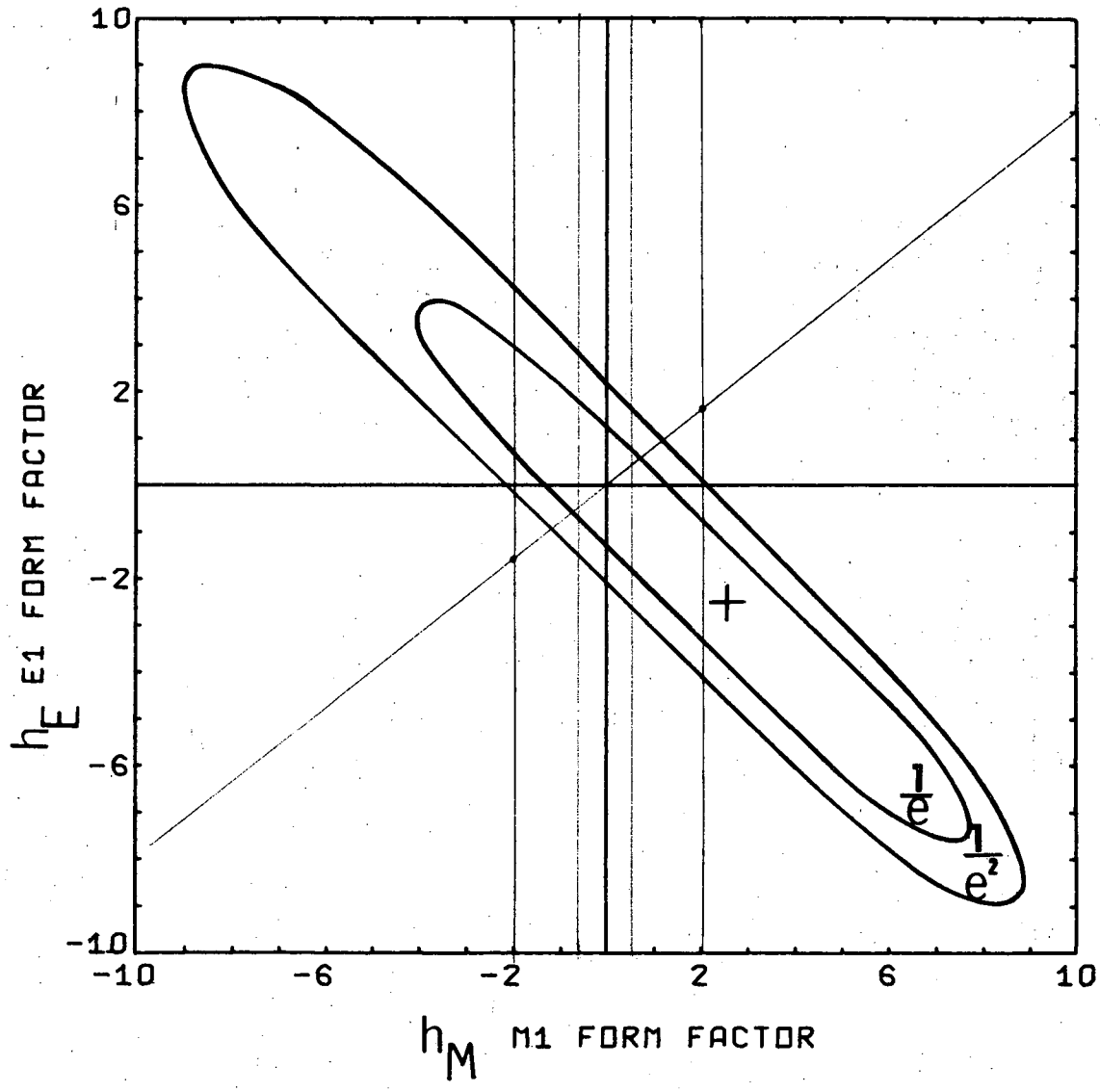


XBL 6812-6406

Fig. 12. Maximum likelihood analysis for fitting the data to the distribution predicted for various values of the E1 and M1 form factors ($h_E$, $h_M$).

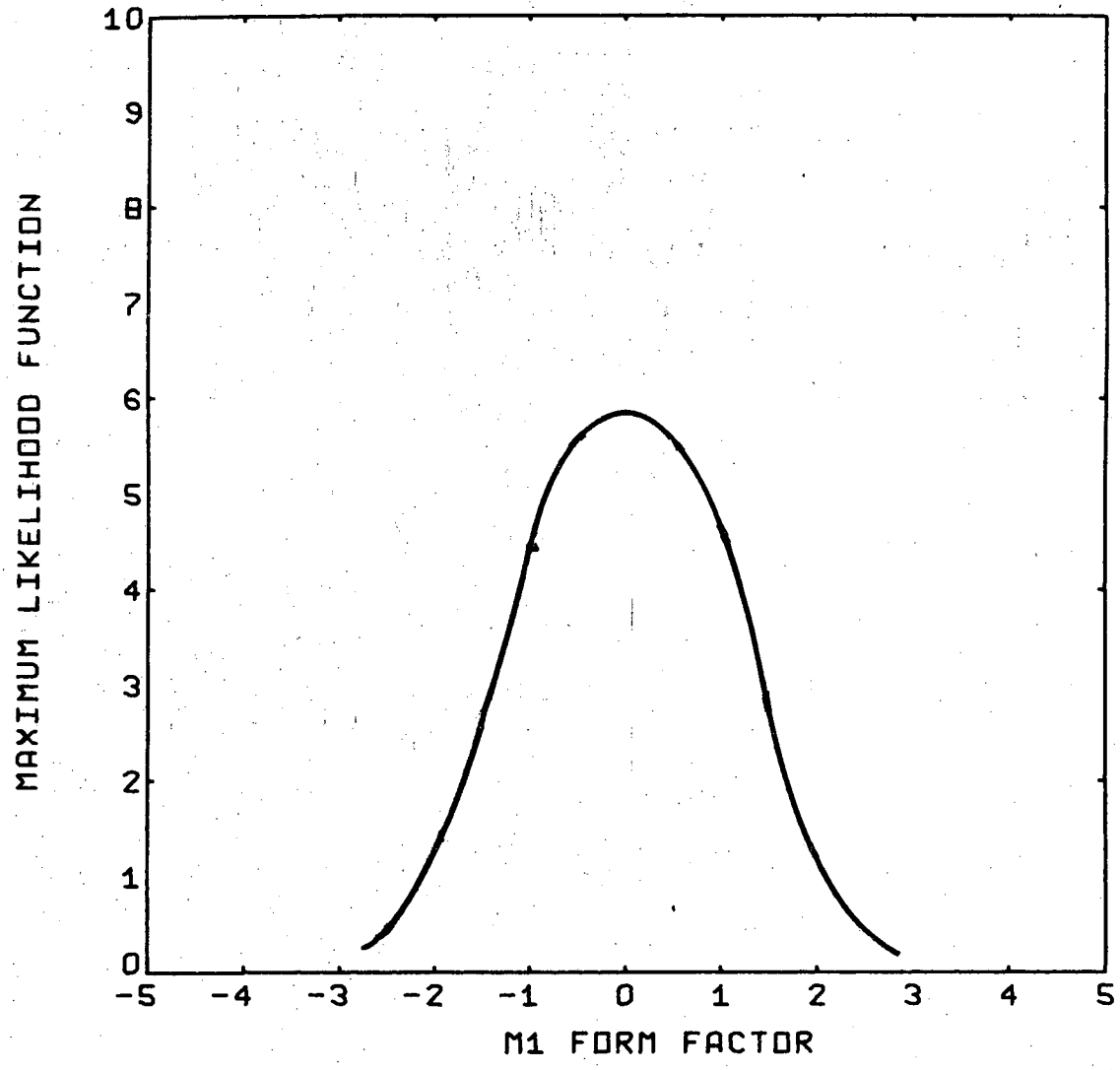


XBL 6812-6407

Fig. 13. Maximum likelihood analysis with respect to the M1 term only, $h_E$ assumed zero.

$h_E$ is negligible. However if there were a spin 1 K* meson with mass below the Kπ threshold, the value of $h_M$ would be greatly enhanced. Our result is incompatible with the existence of such a vector meson. The distribution in cos $\theta_{\mu\gamma}$ of the $K^+ \to \mu^+ + \nu + \gamma$ events that would be detected by our apparatus if the form factor were $h_M = 2.3$ is shown in Fig. 17.

Substituting $h_E$ for $h_M$ in the above equations we did a similar maximum likelihood function analysis with respect to the E1 term only. The result is plotted in Fig. 14. We found $h_E = -0.7^{+1.8}_{-1.1}$ or $|h_E| < 2.9$ at 95% confidence level. If we neglect the dependence on the energy of the gamma ray, the mass of W meson can be related to $h_E$,

$$m_W = \left( \left( (2-\mu_W)/h_E \right) + 1 \right)^{1/2} m_K$$

where $\mu_W$ is the anomaleous magnetic moment of the W meson. For $\mu_W = -2$, we got $m_W > 750$ MeV.

Taking $h_M$ to be 1.5, we made a Monte Carlo program to generate $K^+ \to \mu^+ + \nu + \gamma$ events. The distribution of the generated events in cos $\theta_{\mu\gamma}$ is shown in Fig. 15. The observed data is shown in Fig. 16. none of the 27 events lies in the interval $-1 < \cos\theta_{\mu\gamma} < -0.9$ where more than 66% of the direct decay events should appear (Fig. 15). Assuming there are less than 2.2 $K^+ \to \mu^+ + \nu + \gamma$ events in the interval $-1 < \cos\theta_{\mu\gamma} < -0.9$ due to the direct decay in our sample, we can set an upper limit for the branching ratio of the direct decay of $K^+ \to \mu^+ + \nu + \gamma$ in the spectrum interval $137 < T_\mu < 142$ MeV of $1.1 \times 10^{-5}$ at 90% confidence level. In the same energy interval, the branching ratio of the inner bremsstrahlung is expected to be $1.0 \pm 0.1 \times 10^{-3}$.

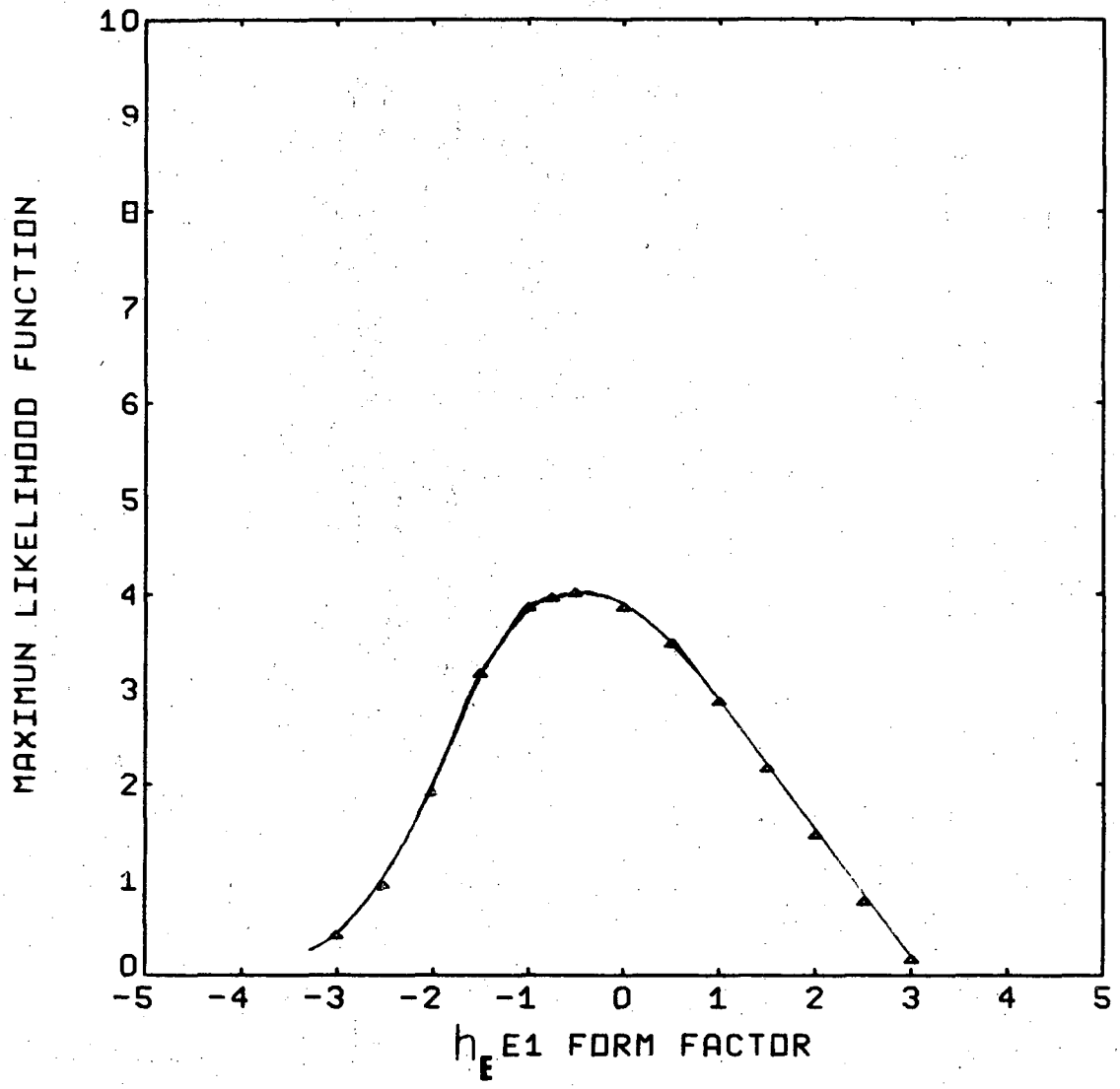


XBL 6812-6453

Fig. 14. Maximum likelihood analysis with respect to the E1 term only, $h_M$ assumed zero.

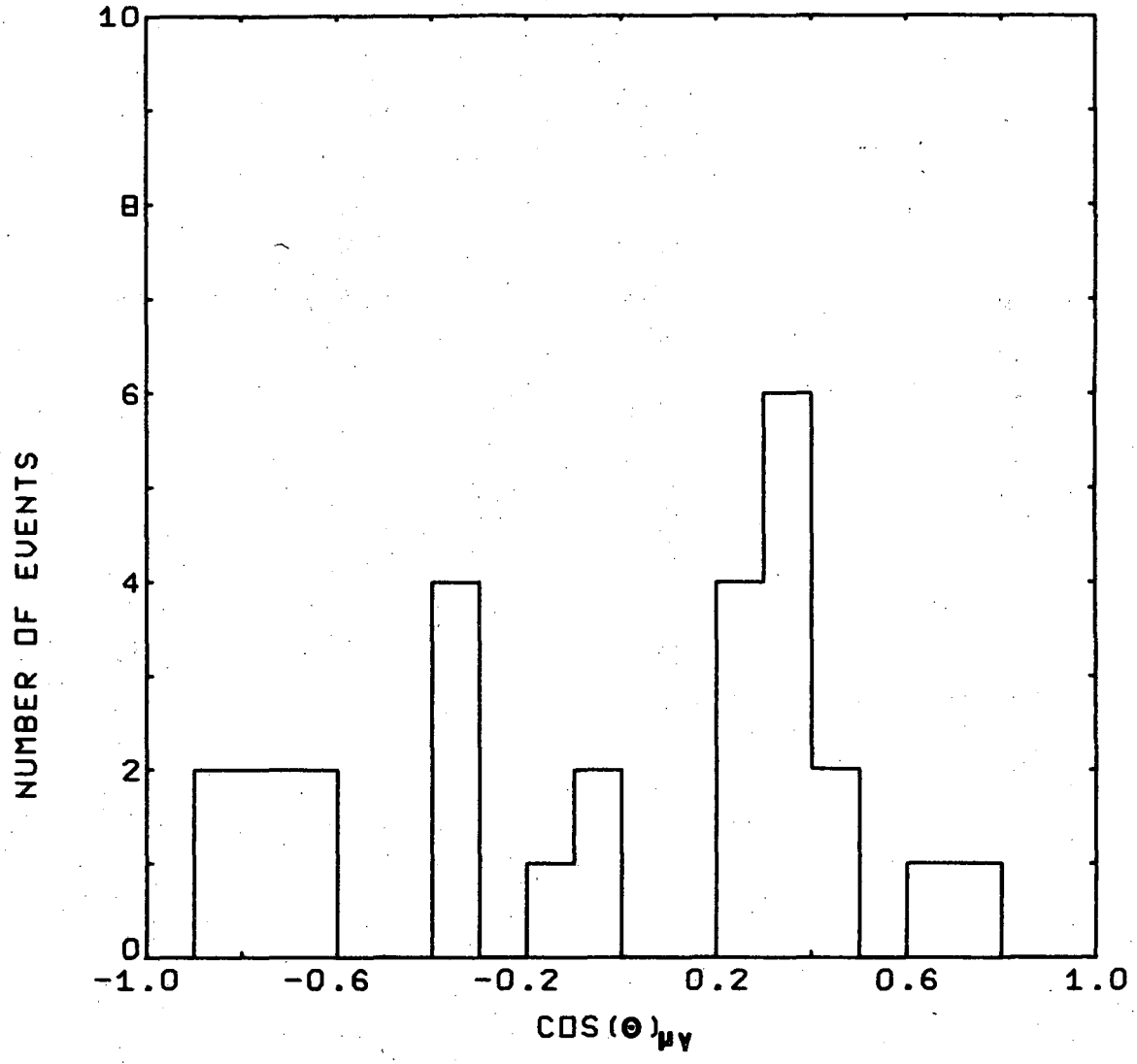


XBL 6812-6345

Fig. 15. Distribution in cos $\theta$ (the angle between the muon and gamma direction) of the decay $K^+ \rightarrow \mu^+ + \nu + \gamma$. Only the sum of the direct term with $h_M = 1.5$, $h_E = 0$ and the interference between this term and the bremsstrahlung term is shown (detection efficiency built in).

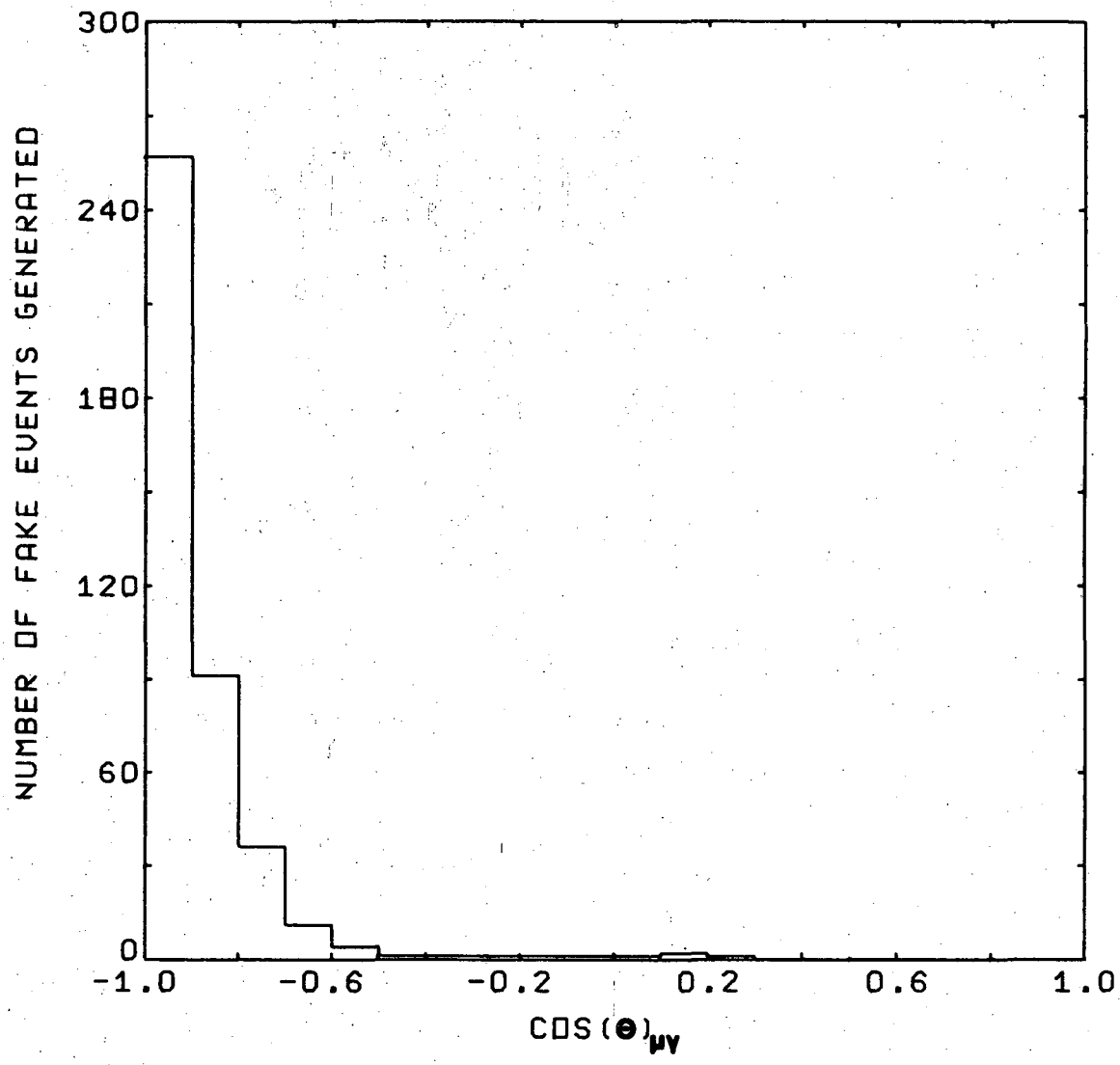


XBL 6812-6344

Fig. 16. Distribution in cos $\theta$ of the data from this experiment.

The uncertainty in the branching ratio is due to one MeV uncertainty in the measured mean muon energy.

As a final check on our efficiency calculation, we have calculated the absolute number of $K^+ \to \mu^+ + \nu + \gamma$ events we should observe in our data. We observed $4.8 \times 10^5$ $K_{\mu 2}$ events. The overall detection efficiency (not including the gamma ray) is calculated to be 41%. Assuming there is only inner bremsstrahlung decay, we expect $228 \pm 24$ $K^+ \to \mu^+ + \nu + \gamma$ events with muon energy between 137 and 142 MeV among which $26 \pm 6$ should be associated with a detected gamma ray. This agrees very well with the 27 events which we found with gamma ray showers.

The significance of our result is that we have set an upper limit of the direct term (Eq. I-2) which turns out to be small. The smallness of the direct decay makes the search of T-violation in this decay impractical. We must stress, however, that our upper limit for the direct decay $K^+ \to \mu^+ + \nu + \gamma$ is still a factor 5 above the rate for inner bremsstrahlung alone for the events with high energy muons and gamma rays emitted in the backward region ($E_\mu \sim 139$ MeV and $\cos \theta_{\mu\gamma} \sim -.9$). Therefore it is of interest to further improve this result by an order of magnitude, to test the theoretical predictions of the direct process.

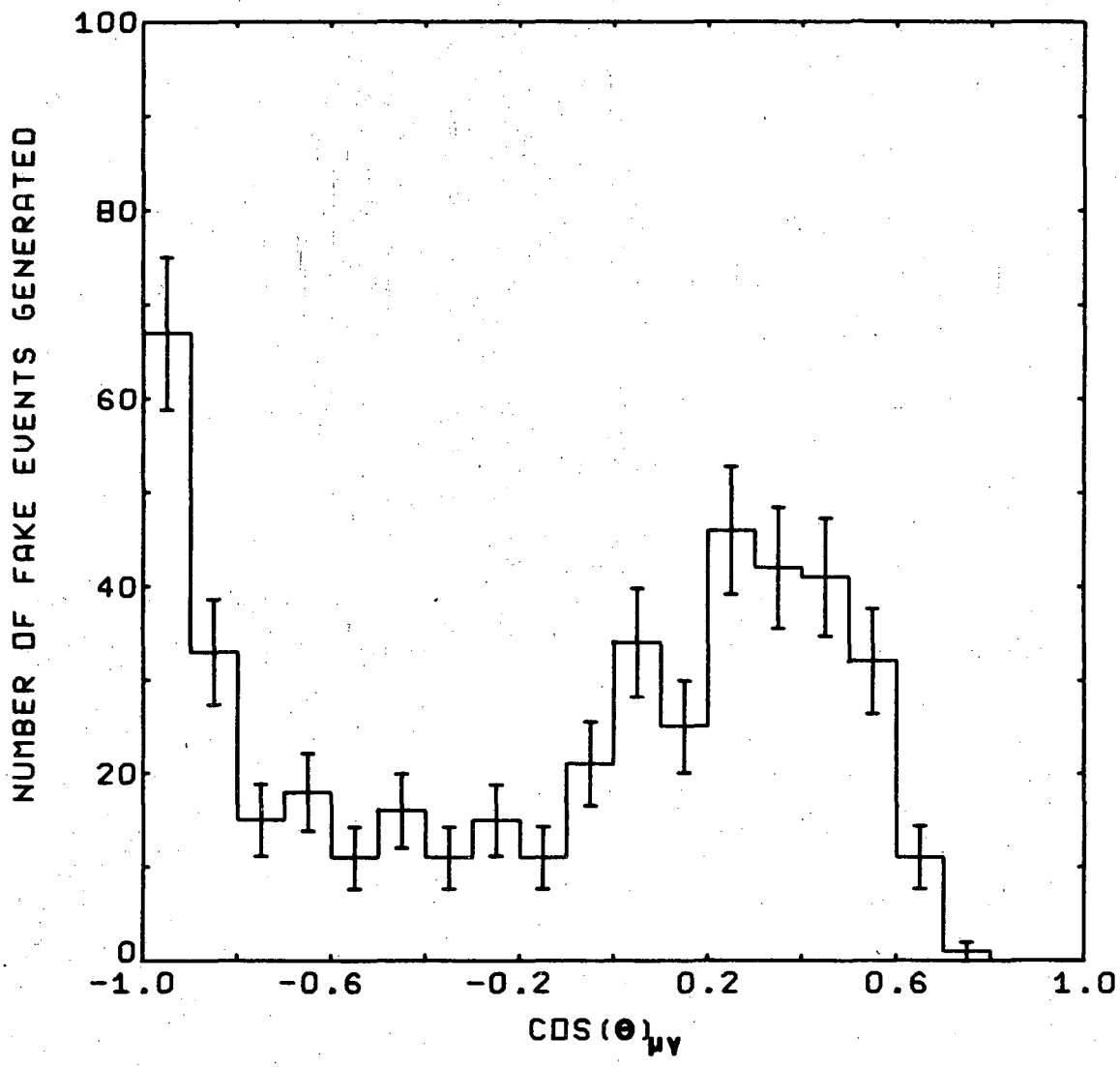


XBL 6812-6342

Fig. 17. Distribution in cos $\theta$ of the $K^+ \rightarrow \mu^+ + \nu + \gamma$ events that would be detected by our apparatus if the form factor $h_M = 2.3$. The detection efficiency has been built in.

## II. SEARCH FOR THE DIRECT DECAY $K^+ \rightarrow \pi^+ + \gamma + \gamma$

### ABSTRACT

We undertook a search for examples of the direct decay mode $K^+ \rightarrow \pi^+ + \gamma + \gamma$ where the invariant mass of the two gamma rays is different from that of the $\pi^o$. Candidates were recognized by the relation of the conversion points of two gamma rays to the momentum of a charged particle. The charged particle was assumed to be a pion. Its momentum was determined from its range in an aluminum plate spark chamber. Our apparatus was sensitive to pions having a kinetic energy between 60 and 90 MeV. The gamma rays were detected by a lead plate spark chamber.

The $K_{\mu 3}$ provided almost the sole background. In 6780 events with good gamma ray showers we found $29 \pm 5.5$ events that fitted the decay $K^+_{\pi\gamma\gamma}$ hypothesis within our energy and spacial resolution. However the expected background was $30 \pm 3$ events. If we assume the hypothetical direct decay process $K^+ \rightarrow \pi^+ + \gamma + \gamma$ to be distributed according to a phase space model, we can set an upper limit for the braching ratio of the $K^+$ into this channel of $1.1 \times 10^{-4}$ at a confidence level of 90%. Following the suggestion of Fujii,[14] we have interpreted our result as a limit on the off-the-mass shell variation of the $K^+ \rightarrow \pi^+ + \pi^o$ amplitude. If this amplitude is assumed to be of the form

$$M(q^2) = M(m^2_{\pi^o})\left(1-\xi \frac{q^2-m^2_{\pi^o}}{m^2_{\pi^o}}\right)$$

our result requires that $|\xi| < 30$. In this expression q is the invariant mass of the two gamma rays. Our results are incompatible with the

suggestion of Lapidus[15] that the $K^+ \to \pi^+ + \gamma + \gamma$ mode may be related to the $\eta \to \pi^o + \gamma + \gamma$ mode through a $\sigma$ meson intermediate state model. The rate of $K^+ \to \pi^+ + \gamma + \gamma$ predicted by Lapidus is more than an order of magnitude greater than what we obtain from our upper limit of the branching ratio.

If we assume that $\Gamma(K_2^o \to \pi^o + \gamma + \gamma)$ approximately equals $\Gamma(K^+ \to \pi^+ + \gamma + \gamma)$ we can set an upper limit for the branching ratio of the decay mode $K_2^o \to \pi^o + \gamma + \gamma$ of $5 \times 10^{-4}$ which is a small number and should not affect the present measurement of the branching ratio of $K_2^o \to \pi^o + \pi^o$ or the quantity $\eta_{oo}$.

## A. INTRODUCTION

### a. General Review

This part of the thesis is based on the result of a spark chamber experiment performed at the Bevatron to search for the decay mode $K^+ \to \pi^+ + \gamma + \gamma$. The decay $K^+ \to \pi^+ + \gamma + \gamma$ is first order in weak interactions and second order in electromagnetic interactions. It can occur by inner bremsstrahlung or by direct emission of the photons through some intermediate particles. However, if we assume the effective weak Hamiltonian to be of the form $\tau\pi^{+*}K^+$ or $\partial_\mu\pi^{+*}\partial_\mu K^+$, it is straightforward to show[14] that all the contributions from $K^+$ and $\pi^+$ currents vanish, i.e. there is no inner bremsstrahlung term in this reaction (Fig. 18).

The direct decay can occur through many intermediate states. Some of the most important ones are shown in Fig. 19. Among them the contribution of the first two diagrams was found[14] to be negligibly small (about $0.3 \times 10^{-7}$). The branching ratio based on Fig. 19c is about $10^{-6}$ if there is no $\pi\pi$ resonance. But if there is a $\pi\pi$ resonance with quantum number $0(0^+)$, i.e. Fig. 19-d, the branching ratio of $K^+ \to \pi^+ + \gamma + \gamma$ was estimated by Lapidus[15] to be of the order of 1% of the total $K^+$ decay. The branching ratio does not depend strongly on the mass and width of the $\sigma$ meson. For a wide range of the $\sigma$ parameters the branching ratio changes from 0.4% to 1%. The diagram in Fig. 19-c was also considered by Lapidus. He concluded that a decay due to this diagram is practically the same as the decay mode $K^+ \to \pi^+ + \pi^0$ because of the small width of the $\pi^0$ meson. Cabibbo and Gatto[17] introduced a derivative coupling for the decay $K^+ \to \pi^+ + \pi^0$.

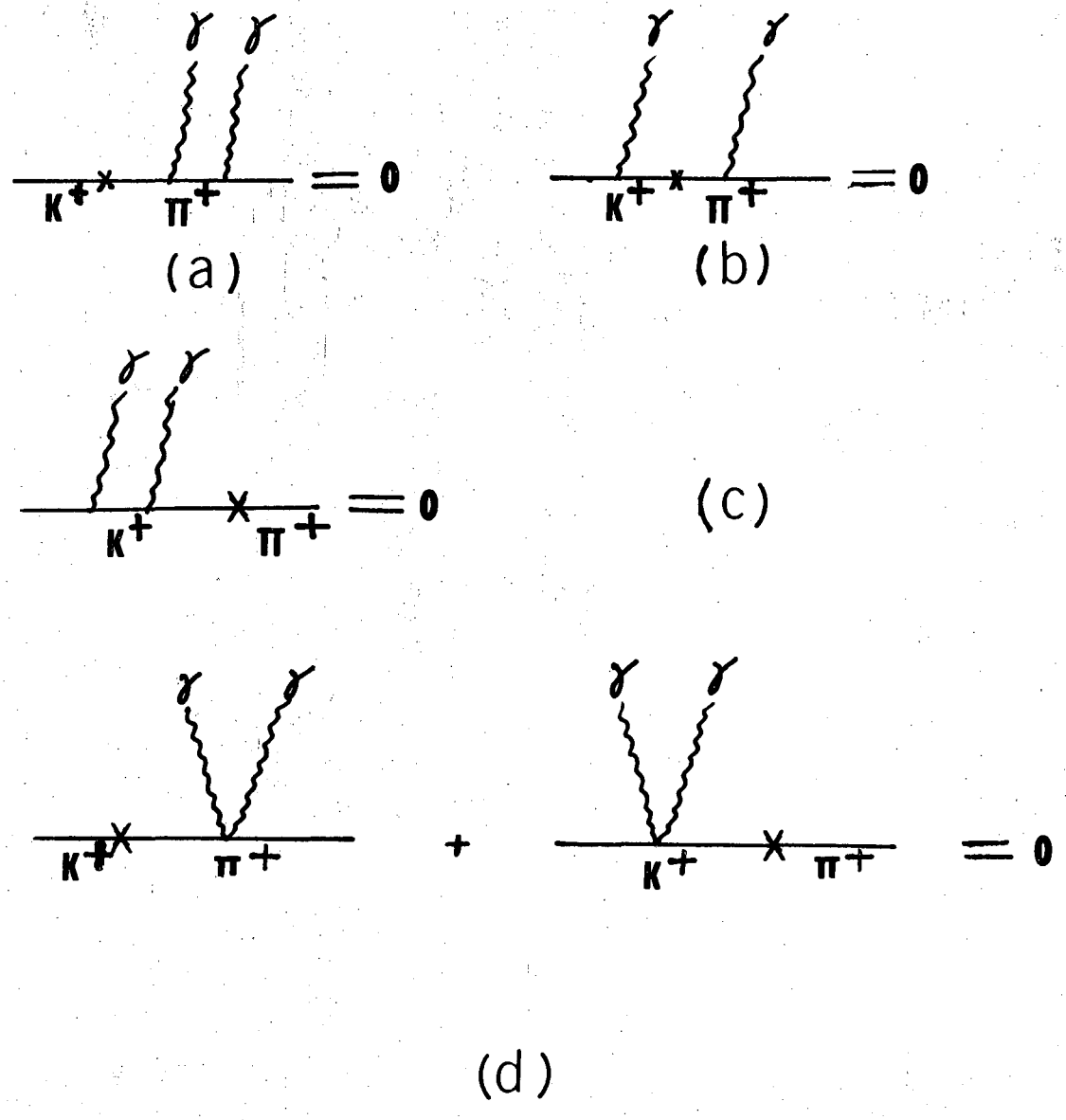


XBL 6812-6341

Fig. 18. Feynman diagrams for the inner bremsstrahlung of the decay $K^+ \to \pi+\gamma+\gamma$. The contribution of the inner bremsstrahlung vanishes.

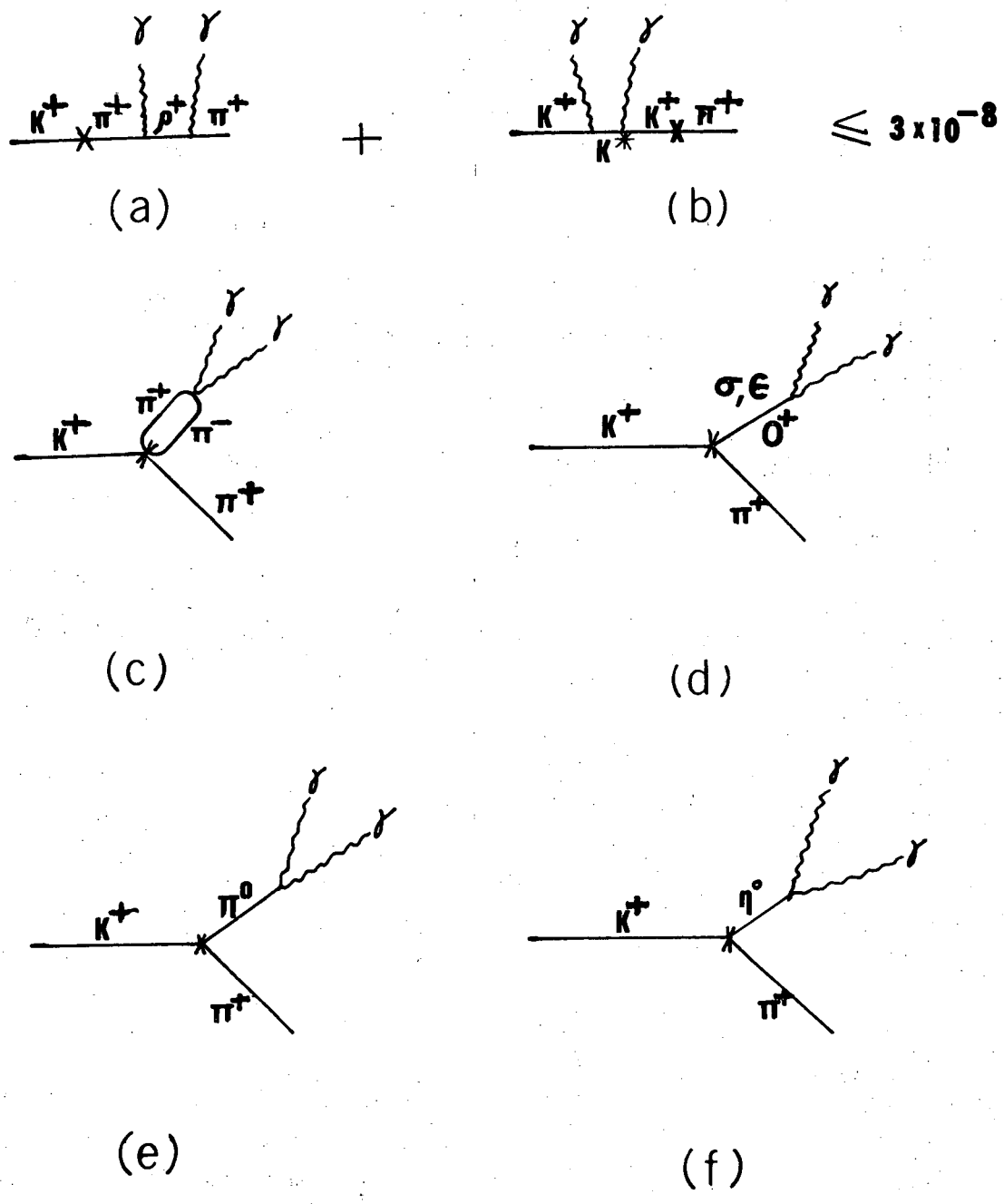


XBL 6812-6340

Fig. 19. Feynman diagrams of various direct processes for the decay $K^+ \to \pi^+ + \gamma + \gamma$.

Fujii,[14] assuming the decay $K^+ \to \pi^+ + \gamma + \gamma$ is dominated by the same diagram but with the derivative coupling, predicted the branching ratio to be around $6 \times 10^{-5}$ of the total $K^+$ decay. We will furthur discuss this model in (b).

b. The Decay $K^+ \rightarrow \pi^+ + \gamma + \gamma$ as a Test of the $\Delta I = 1/2$ Rule in the Weak Interactions

The mechanism causing the $K^+ \rightarrow \pi^+ + \pi^o$ decay has been the subject of considerable theoretical speculation. Under the assumption[29] that angular momentum is conserved in weak interactions, we can deduce the spin of the $K^+$ meson from the distribution of its decay particles in the Dalitz plot. The fact that the Dalitz plot of the decay $K^+ \rightarrow \pi^+ + \pi^- + \pi^+$ is flat and uniformly distributed strongly suggests that the spin of the $K^+$ meson is zero. The relative orbital angular momentum, L, of the two $\pi$-mesons in the decay $K^+ \rightarrow \pi^+ + \pi^o$ should equal the spin of the $K^+$ meson. The parity of the two $\pi$-mesons in the final state is $(-1)^L$ which is even when L=0. Bose statistics would require that the wave function be symmetric under the interchange of two $\pi$-mesons if the pions were identical. This obtains if we describe the different pions as the same particle with an isotopic spin and a different third component of isospin. However in this approximation the masses of the pions should be identical. This is not the case for charged and neutal pions and the electromagnetic interaction breaks the symmetry that would allow the description of the pions by a different $I_Z$ only. Let us first assume that the charged and neutral pions are identical with the understanding that the relative magnitude of the correction term involved here could be as large as the square of the ratio of the mass difference to the mass of the pion. The even spacial wave function then implies the isotopic spin wave function must also be even. With the conventional notation $|1,1> = \pi^+$, $|1,0> = \pi^o$, $|1,-1> = \pi^-$, the isotopic spin

wave functions of two pion mesons are as follows:

$$|2,1\rangle = \frac{1}{\sqrt{2}} [|\pi^+,\pi^o\rangle + |\pi^o,\pi^+\rangle] ,$$

$$|2,0\rangle = \frac{1}{\sqrt{6}} [2|\pi^o,\pi^o\rangle + |\pi^+,\pi^-\rangle + |\pi^-,\pi^+\rangle] ,$$

$$|1,1\rangle = \frac{1}{\sqrt{2}} [|\pi^+,\pi^o\rangle - |\pi^o,\pi^+\rangle] , \qquad \text{(II-1)}$$

$$|1,0\rangle = \frac{1}{\sqrt{2}} [|\pi^+,\pi^-\rangle - |\pi^-,\pi^+\rangle] ,$$

$$|0,0\rangle = \frac{1}{\sqrt{3}} [|\pi^+,\pi^-\rangle + |\pi^-,\pi^+\rangle - |\pi^o,\pi^o\rangle | .$$

The I=0 state is not available for the two-pion system from $K^+$ decay because the relation $I_Z=Q$ together with charge conservation requires I greater than or equal to 1.

From (II-1), we see that the I=1 state is odd and the I=2 and I=0 states are even under the interchange of the isotopic coordinates of the two $\pi$-mesons. Therefore if we assume that the electromagnetic interaction in the decay mode $K^+ \to \pi^+ + \pi^o$ is negligible we find that isotopic spin of the final state in the decay $K^+ \to \pi^+ + \pi^o$ is 2 while that of the $K^o \to \pi^+ + \pi^-$ decay is 0 (or 2). As the isotopic spin of the K meson is 1/2, it follows that the smallest possible change of the isotopic spin in $K^+ \to \pi^+ + \pi^o$ decay is 3/2 and that in the $K^o \to \pi^+ + \pi^-$ is 1/2. If the $\pi^+\pi^o$ final state in the $K^+$ decay were a pure isospin 2 state, and if the weak interaction satisfied the $|\Delta I| = 1/2$ law exactly, this decay would be forbidden. Indeed, the amplitude for this decay is about twenty times smaller than the amplitude for the $K^o \to 2\pi$ decay which does not violate the $|\Delta I| = 1/2$ selec-

tion rule. Since $\Delta I=1/2$ rule is generally obeyed in weak nonleptonic decays it is of interest therefore to attempt to determine the actual mechanism through which the $K^+ \to \pi^+ + \pi^o$ decay occurs.

It was suggested by Gell-Mann and Pais[13] and Cabibbo[30] that the decay $K^+ \to \pi^+ + \pi^o$ may occur because of the presence of electromagnetic interactions. Thus the $2\pi$ final state may not be a pure isospin state on account of the $\pi^+$, $\pi^o$ mass difference which is likely caused by electromagnetic interactions. The advantage of this kind of model lies in the analogy between the relation of strong ($\Delta I=0$) and electromagnetic ($\Delta I=1,0$) interactions and the relation of $\Delta I=1/2$ and the $\Delta I=3/2$ interactions. In general, all measurable violations of the $\Delta I=1/2$ rule in the weak strangeness changing decays should be due to electromagnetic corrections.[30]

Let f and g denote the weak coupling constants between hadrons when the decay vertex obeys or violates the $\Delta I=1/2$ rule respectively. Following Cabibbo and Gatto[17] we can assume that the decay $K^+ \to \pi^+ + \pi^o$ occurs through the following Lagrangian:

$$\mathcal{L}'' = g\, m_K^3\, \Phi_+\, \varphi_+^*\, \varphi_o + H.C. \qquad \text{(II-2)}$$

where $m_K$ is the $K^+$ mass, $\Phi_+$ is the $K^+$ field and $\varphi_+$, $\varphi_o$ are the charged and neutral pion fields respectively. Since the space wave function is even, the two pions must be in an I=2 state. Therefore this process necessarily violates the $\Delta I=1/2$ rule. Now if one of the emitted $\pi$ mesons is a virtual particle with a mass different from the mass of the other $\pi$ meson, we can introduce another Lagrangian such that the space wave function of the two mesons is odd. The isotopic wave function

is necessarily also odd to make the total wave function even. The simplest Lagrangian corresponding to the decay $K^+ \to \pi^+ + \pi^o$ (virtual) which satisfies the $\Delta I=1/2$ rule is:

$$\mathcal{L}' = \sqrt{2}\ \tau\ m_K \frac{\partial \Phi_+}{\partial X_\nu}\ \varphi_+^* \left( \frac{\vec{\partial}}{\partial X_\nu} - \frac{\vec{\partial}}{\partial X_\nu} \right) \varphi_o \ + \text{H.C.} \qquad \text{(II-3)}$$

If we evaluate $\mathcal{L}'$ in the rest system of the $K^+$ meson, we find that $\mathcal{L}'$ is proportional to $(E_{\pi^+} - E_{\pi^o})$ which vanishes in the case that the masses of the two pions are the same and is proportional to the difference of the square of the masses of the two pions. The coupling constant f can only be defined on the basis of a model for K decays. Following Cabibbo and Gatto, we assume that the decay $K^o \to \pi^+ + \pi^-$ occurs, similar to the process corresponding to $\mathcal{L}'$, from the following Lagrangian:

$$\mathcal{L}'\ (K^o \to 2\pi) = f\ m_K \frac{\partial \Phi_o}{\partial X_\nu}\ (\vec{\varphi} \cdot \frac{\partial \vec{\varphi}}{\partial X_\nu}) \qquad \text{(II-4)}$$

The value of f can be obtained by comparing the above expression with the measured $K^o \to \pi^+ + \pi^-$ decay rate. Experimentally we know that the amplitude which violates $\Delta I=1/2$ rule is severely suppressed, i.e. g is much smaller than f.

There are two $K^+$ meson decay modes where one of the pions in the final state is off mass shell.

(1) $K^+ \to \pi^+ + \pi^o + \gamma$ . The total amplitude consists of an internal bremsstrahlung and of a direct amplitude. If there is a large off-mass-shell effect ($\mathcal{L}'$), the direct amplitude will contain a process

$$K^+ \to \pi^+ + \pi^o$$
$$\qquad\quad \downarrow$$
$$\qquad\quad \pi^+ + \gamma$$

where the intermediate $\pi^+$ is off the mass shell. The decay vertex $K^+ \to \pi^+ + \pi^o$ therefore satisfies $\Delta I=1/2$ rule.

At first glance, the conjecture that the amplitude becomes large off the mass shell may appear to be in contradiction to the experimental observation that the radiative decay $K^+ \to \pi^+ + \pi^o + \gamma$ occurs with the frequency of ordinary inner bremsstrahlung. If the $K^+ \to \pi^+ + \pi^o$ amplitude is due to an electromagnetic correction to the weak interaction, and is therefore of order $e^2$, one might think that the $K^+ \to \pi^+ + \pi^o + \gamma$ amplitude, which would be of order e, would be large in comparison with the non-radiative amplitude. Experimental results, however, indicate that this is not so.

It was shown[17] that $\mathcal{L}'$, even with a large off-the-mass shell $\Delta I=1/2$ coupling constant f, will not give rise to abundant radiative decay. In fact, the contribution of $\mathcal{L}'$ vanishes[17] in this decay when we require the decay matrix to be gauge invariant. Therefore we find the off-the-mass shell effect will not show up in this decay mode.

(2) $K^+ \to \pi^+ + \pi^o$ where the mass of the virtual $\pi^o$ is different from that of the $\pi^+$ meson. $\pi^o \longrightarrow \gamma + \gamma$ This reaction is investigated in the present experiment.

Many authors[14,18,19,27] have also come to the conclusion that the $K^+ \to \pi^+ + \pi^o$ amplitude may become very large when the $\pi^o$ is not on the mass shell by applying current algebra to non-leptonic K meson decays. The same conclusion was reached by Sakurai[28] using a simple dynamical model of vector meson dominance. Fujii further assumed that the $K^+ \to \pi^+ + \gamma + \gamma$ process is dominated by a single diagram in which there is a $\pi^o$ intermediate state and that the amplitude for $K^+ \to \pi^+ + \pi^o$

varies in the following manner:

$$M(q^2) = M(m_{\pi^o}^2)\left(1 - \xi \frac{q^2 - m_{\pi^o}^2}{m_{\pi^o}^2}\right) \qquad \text{(II-5)}$$

In this expression, $M(m_{\pi^o}^2)$ is the on-mass-shell amplitude for $K^+ \to \pi^+ + \pi^o$ decay, $m_{\pi^o}$ is the mass of $\pi^o$; q is the invariant mass of the two gamma rays and $\xi$ is related to the coupling constants f and g by

$$\xi = \frac{\sqrt{2}\, f m_{\pi^o}^2}{g m_K^2 + \sqrt{2}\, f(m_{\pi^+}^2 - m_{\pi^o}^2)} \quad .$$

Cabibbo and Gatto, and Fujii have related the parameter $\xi$ to the amplitude for $K_s^o \to \pi^+ + \pi^-$ decay. Fujii finds that,

$$|\xi| \cong \frac{M(K^o \to \pi^+ + \pi^-)}{M(K^+ \to \pi^+ + \pi^o)} \cong 20 \qquad \text{(II-6)}$$

and in the model of Okubo et al.[19] we find

$$|\xi| = \frac{m_{\pi^o}^2}{m_{\pi^+}^2 - m_{\pi^o}^2} = 14 \quad .$$

In order to compare our results with the above predictions, we have calculated the differential spectrum of the $\pi^+$ energy in the $K^+ \to \pi^+ + \gamma + \gamma$ decay for various values of $\xi$. The result is as follows:

$$\frac{1}{\Gamma(K^+ \to \pi^+ + \pi^o)} \frac{d\Gamma(K^+ \to \pi^+ + \gamma + \gamma)}{dE_{\pi^+}} =$$

$$\frac{2}{\pi} \frac{M_K}{m_{\pi^o}^3} \Gamma(\pi^o \to 2\gamma) \frac{P_\pi^+}{P_o} q^4 \left| \frac{1}{q^2 - m_{\pi^o}^2 - i m_{\pi^o} \Gamma(\pi^o \to 2\gamma)} - \frac{\xi}{m_{\pi^o}^2} \right|^2 \qquad \text{(II-7)}$$

In this expression $P_\pi^+$ is the momentum of the $\pi^+$ in $K^+ \to \pi^+ + \gamma + \gamma$ decay, while $P_o$ is the momentum of the $\pi^o$ in the decay $K^+ \to \pi^+ + \pi^o$. For the purpose of comparing this calculation with our experimental results we have assumed that $\Gamma(\pi^o \to 2\gamma) = 7.4 \pm 0.15 \times 10^{-6}$ MeV as given in the table of Rosenfeld et al.[21] Since $\Gamma(\pi^o \to 2\gamma) << m_{\pi^o}$, the term $q^2 - m_{\pi^o}^2$ completely dominates over the term $m_{\pi^o}\Gamma(\pi^o \to 2\gamma)$ when $q^2$ is sufficiently different from $m_{\pi^o}^2$. Therefore even though $\Gamma(\pi^o \to 2\gamma)$ can vary as $q^3$, the energy dependence of $\Gamma(\pi^o \to 2\gamma)$ will not affect the predicted differential rate. Several distribution curves in the kinetic energy of the pion corresponding to different positive values of $\xi$ are shown in Fig. 20. Using $\xi = 20$ we find the predicted branching ratio for the decay mode $K^+ \to \pi^+ + \gamma + \gamma$ with $E_{\pi^+} < 90$ MeV is $6 \times 10^{-5}$. The predicted branching ratio for $\xi = -20$ is about 6% greater than that of $\xi = 20$. Therefore it is interesting to look for the decay $K^+ \to \pi^+ + \gamma + \gamma$ to test this and other theoretical models mentioned in the general review (a).

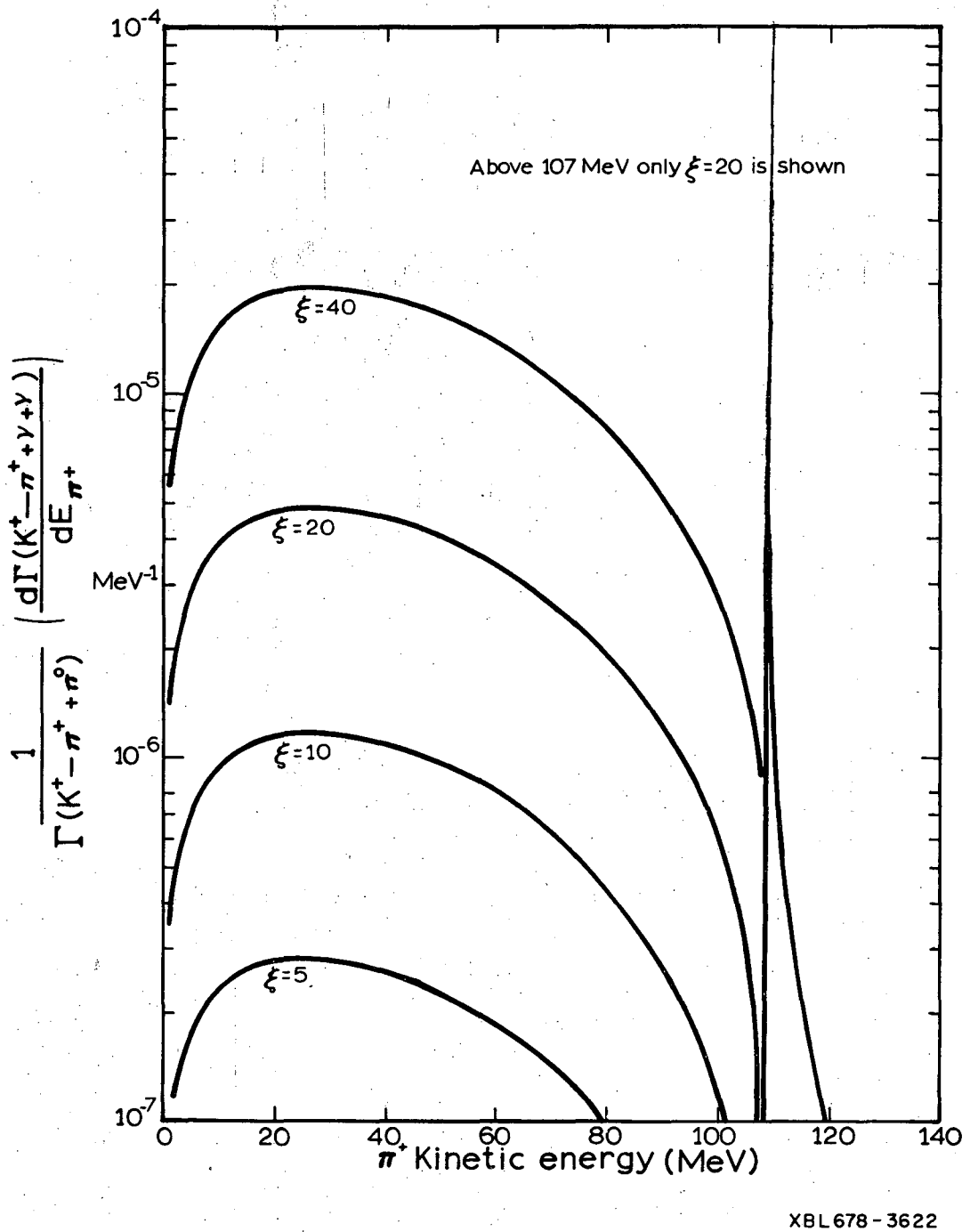


Fig. 20. Distribution in the energy of the pion of the decay $K^+ \to \pi^+ + \gamma + \gamma$ as predicted by the off-the-mass shell model. The predicted branching ratio of this decay with pion energy below 90 MeV is $6 \times 10^{-5}$. $\xi$ is defined in the text.

## B. APPARATUS

The beam set up and spark chamber--counters system were mainly the same as that used in the $K^+ \rightarrow \mu^+ + \nu + \gamma$ experiment (Figs. 3, 4 and Fig. 5).

The kaon stopper at the center of Fig. 5, which consisted of a scintillation counter box filled with carbon dust, was placed at the second focus of a 500 MeV/c single-stage separated $K^+$ beam at the Bevatron. $K^+$ mesons, which entered the apparatus in a direction perpendicular to the figure, were identified by a variety of scintillation counters and a Cerenkov counter in the beam. The counting system is not shown in the figure. There were two spark chambers in the $K^+$ beam immediately before the stopper to assist in the determination of the stopping point of the K meson.

The set of counters T2, T3, $\bar{C}$, T4, and $\overline{T5}$, which we called the pion telescope, was used to identify charged particles from $K^+$ decay.

The spark chamber trigger requirement was a T2-T3-T4-$\bar{C}$-$\overline{T5}$ fast coincidence occurring in the interval from $6\text{-}35 \times 10^{-9}$ seconds after a K-stop signal. The water Cerenkov counter in the pion telescope served to reject electrons from the $K^+_{e3}$ decay mode, and products of gamma ray conversions. Pions with insufficient energy to go beyond the $\overline{T5}$ anti-coincidence counter were not detected in the Cerenkov anticoincidence counter. The aluminum degrader shown in the figure was variable and could be adjusted to make the range interval between T4 and $\overline{T5}$ correspond to an initial pion kinetic energy from 50 to 150 MeV. The degraders used in detecting different $K^+$ decay modes were listed below:

| | Degrader | Decay particle | K.E. Spectrum accepted |
|---|---|---|---|
| $K^+ \rightarrow \pi^+ + \gamma + \gamma$ (I) | 6.9 gm/cm$^2$(Al) | $\pi^+$ | 70 → 90 MeV |
| $K^+ \rightarrow \pi^+ + \gamma + \gamma$ (II) | 2.59gm/cm$^2$(Al) | $\pi^+$ | 60 → 80 MeV |
| $K^+ \rightarrow \pi^+ + \pi^o$ | 19 gm/cm$^2$ (Al) | $\pi^+$ | 100 → 117 MeV |
| $K^+ \rightarrow \mu^+ + \nu$ | 6.9 gm/cm$^2$(Al) | $\mu^+$ | 143 → 158 MeV |
| | 47 gm/cm$^2$ (Cu) | | |

The pion range spark chambers were fired 3.5 μs after the electronic system was triggered so that the μ-e decay was recorded for the purpose of measuring the decay $K^+ \rightarrow \mu^+ + \pi^o + \nu$ in the experiment of Cutts et al. The clearing voltage for the pion range spark chambers was changed to 6.6 volts in order to maintain the tracks in those chambers for as long as 3.5 μs.

The average beam rate was lower than that of the $K^+ \rightarrow \mu^+ + \nu + \gamma$ experiment in order to be compatible with other experiments running simultaneously at the Bevatron. The $K^+$ stop rate ranged from 400 to 1000 per Bevatron pulse. The trigger rate was about once per five Bevatron pulses.

As before, the delayed $K^+$ decay is defined to be:

$$K(\text{delayed decay}) = (S1\text{-}S2\text{-}S3\text{-}S4\text{-}\bar{C}_k\text{-}\bar{S}_5)\text{-}(T2\text{-}T3\text{-}T4\text{-}\bar{C}_e\text{-}\bar{T}_5)_{\text{delayed}} \qquad \text{(II-8)}$$

where all S's and T's are scintillantion counters and C's are Cerenkov counters defined in Section (I-C.).

We observed $5.1 \times 10^6$ delayed $K^+$ decays with degrader I and $0.88 \times 10^6$ delayed $K^+$ decays with degrader II in the three months of running at the Bevatron.

## C. DATA REDUCTION

A total of 90,000 pictures were taken during the running of the Bevatron. All 16 views of the spark chamber system except the two views of the pion range spark chambers were scanned with SPASS, the automatic scanning device. Two percent of the pictures were missed by SPASS and the events were discarded.

From the result of this scanning we obtained the positions and directions of the $K^+$ track and the $\pi^+$ track, the conversion points of the gamma rays and the blackening associated with each shower.

If there were two or more tracks in either of the $K^+$ tracking chambers or the $\mu^+$ tracking chambers, the event was discarded. If either the $K^+$ track or the $\mu^+$ track was missing the event was also discarded. Twenty-three percent of the pictures were discarded because of the above criterion. Five percent of the remaining events were discarded either because of the minimum distance between the $K^+$ track and the $\pi^+$ track was greater than 1 cm or because the calculated $K^+$ stop position was outside the $K^+$ stopper.

Six percent of the remaining events were discarded because there was a charged particle detected by $S_5$ which surrounded the $K^+$ stopper in coincidence with the pion stopped in the range chamber. These charged paricles were possibly due to either gammas converted inside the stopper or a second charged pion from the decay mode $K^+ \rightarrow \pi^+ + \pi^- + \pi^+$. The conversion probability of a single gamma ray inside the stopper was estimated to be 3%.

The pion track was measured in the three tracking chambers SC1, SC2, SC3. In order to eliminate particles decaying in flight and the

scattered particles we required the cosine of the angle defined by the initial and the final direction of the charged particle in the tracking chambers to be greater than 0.998. Fifteen percent of the remaining events were discarded due to this criterion.

If the event satisfied $K_{\pi 2}$ kinematics it was also discarded. With the measured initial charged pion direction and the directions of each gamma ray we transformed the gamma-ray directions in the $\pi^o$ center-of-mass system assuming this event to be a $K_{\pi 2}$ decay. We required the dot product of the two unit vectors along the two gamma-ray directions in the $\pi^o$ rest frame to be greater than -.98. By doing so we discarded more than 95% of the scattered $K_{\pi 2}$ events without losing more than 1% of the $K_{\pi\gamma\gamma}$ decay events.

We selected 11,500 events with two possible gamma-ray showers and unambiguous $K^+$ and $\pi^+$ tracks to be hand-scanned for the direction of the $\pi^+$ track, the position of the $\pi^+$ stop and the pion range on the SCAMP machine at LRL.

Because this sample was chosen primarily for the investigation of a $K_{\mu 3}$ polarization experiment, we discarded most of the events which did not show μ-e decay in the range chamber. Furthermore, if the electron decay direction was within a forward cone of half angle $\theta=\cos^{-1} 0.9$ with respect to the initial muon direction the event was rejected. If the μ-e vertex position was in the counter T4 the event was also rejected. Thirty-four percent of the events were discarded because of the absence of the μ-e decay. Seventy-seven percent of the pions which had reached the end of their ranges would cascade into electrons through the processes $\pi^+ \rightarrow \mu^+ + \nu$ and $\mu^+ \rightarrow e^+ + \nu + \bar{\nu}$. The

electrons of 5% of those with a μ-e decay were in the forward cone and the events were rejected. This accounted for 28% loss of the total events. The remainder were lost due to π-nucleus interactions and inelastic scatterings. Most of the pions came from the decay mode $K_{\pi 2}$.

Finally we were left with 6780 $K^+ \rightarrow \pi^+ + \gamma + \gamma$ candidates. They were ready for a two constraint fit to $K^+ \rightarrow \pi^+ + \gamma + \gamma$ kinematics. We have summarized the procedure of data reduction in Table III.

Table III. Summary of the data reduction for $K^+ \to \pi^+ + \gamma + \gamma$ experiment.

| | | Degrader I | | | Degrader II | | |
|---|---|---|---|---|---|---|---|
| | Delayed $K^+$ decays | $5.1 \times 10^6$ | | | $0.88 \times 10^6$ | | |
| | | $N_i^{(1)}$ | | $N_i^{(1)}/N_{i-1}^{(1)}$ | $N_i^{(2)}$ | | $N_i^{(2)}/N_{i-1}^{(2)}$ |
| 1) | Number of pictures taken | $82 \times 10^3$ | | | $13.2 \times 10^3$ | | |
| 2) | SPASS scanning | $80 \times 10^3$ | or | 98% | $12.9 \times 10^3$ | or | 98.7% |
| 3) | One and only one track in the $K^+$ and the $\pi^+$ tracking chambers | $62.9 \times 10^3$ | Or | 79.1% | $9.75 \times 10^3$ | or | 75.8% |
| 4) | Events selected to be hand scanned | 10789 | or | 17.2% | 1704 | or | 17.5% |
| 5) | Events scanned | 9820 | or | 91% | 1649 | or | 97% |
| | Total Events Scanned (Block I and Block II) | $= N_5^{(1)} + N_5^{(2)}$ | | | $= 11469$ events | | |
| | Events with two converted gamma ray showers | | | | 6780 | or | 59% |

## D. DATA ANALYSIS

From the scanning result with SPASS and with SCAMP we obtained the following information for each event:

1) The position of the $K^+$ decay.

2) The range of the charged particle from the $K^+$ decay.

3) The direction of the decay particle.

4) The position of the conversion points of the two gamma rays.

From the conversion point of each gamma ray and the $K^+$ decay position we determined the unit vector in the direction of that gamma ray.

The energy of the charged decay particle was calculated from the range of that particle by assuming it was a pion or a muon. The calculated energy was then calibrated with the pion kinetic energy of $K_{\pi 2}$ and with the muon kinetic energy of $K_{\mu 2}$ which are known to be 108.6 and 152.5 MeV respectively. The spectrum of measured pion kinetic energy is shown in Fig. 21. The only difference between the $K_{\pi 2}$ run and the $K_{\pi\gamma\gamma}$ run was a piece of degrader of thickness of 12 $gm/cm^2$ aluminum. Therefore the $K_{\pi 2}$ data served as a calibration for the detection efficiencies of the charged decay particle and the two gamma rays.

We took the range and direction of the charged particle in the pion telescope and the direction of one of the gamma rays and computed the expected direction of the second gamma ray. This direction is uniquely predicted if the event is an example of $K^+ \rightarrow \pi^+ + \gamma + \gamma$. We compute the angle $\alpha$ between the predicted direction and the measured direction of the second gamma ray. The angle $\alpha$, however, strongly depends on

the angle $\theta_1$, between the muon direction and the first gamma ray. To make the analysis more symmetric with respect to the two gamma rays and to make the angle $\alpha$ less dependent on $\theta_1$, we then repeat the procedure using the second gamma ray to predict the direction of the first one. We use the average of the angles $\alpha$ from these two computations as a measure of the deviation from $K^+ \rightarrow \pi^+ + \gamma + \gamma$ kinematics.

In order to show that our apparatus would be sensitive to $K^+ \rightarrow \pi^+ + \gamma + \gamma$ events, we adjusted the amount of degrader in the pion telescope so that 108.6 MeV pions from the reaction $K^+ \rightarrow \pi^+ + \pi^o$ would stop between $T^4$ and $\overline{T_5}$. The distribution in cos $\alpha_{av}$ of these events is shown in Fig. 22.

Figure 23 shows the distribution in cos $\alpha_{av}$ that we observe when we reduce the amount of degrader in the pion telescope in order that pions from the reaction $K^+ \rightarrow \pi^+ + \pi^o$ cannot stop in the range interval between $T^4$ and $\overline{T_5}$. During the course of the experiment the degrader was varied so that the pion energy interval from 60 to 90 MeV was covered. There is evidently no peak at cos $\alpha_{av}$=1 in our data.

Several closely related Monte Carlo calculations were made on the CDC 6600 computer to generate fake $K^+ \rightarrow \pi^+ + \gamma + \gamma$ events. The $K^+$ decay point was picked randomly inside the stopper. The direction of the $\pi^+$ was generated according to the observed angle distribution of the charged particle. The directions of the gamma rays were generated based on the following models:

(1) Phase space distribution function:

$$\frac{d\Gamma(K^+ \rightarrow \pi^+ + \gamma + \gamma)}{dE_\pi} = \lambda \, P_{\pi^+} \qquad \text{(II-9)}$$

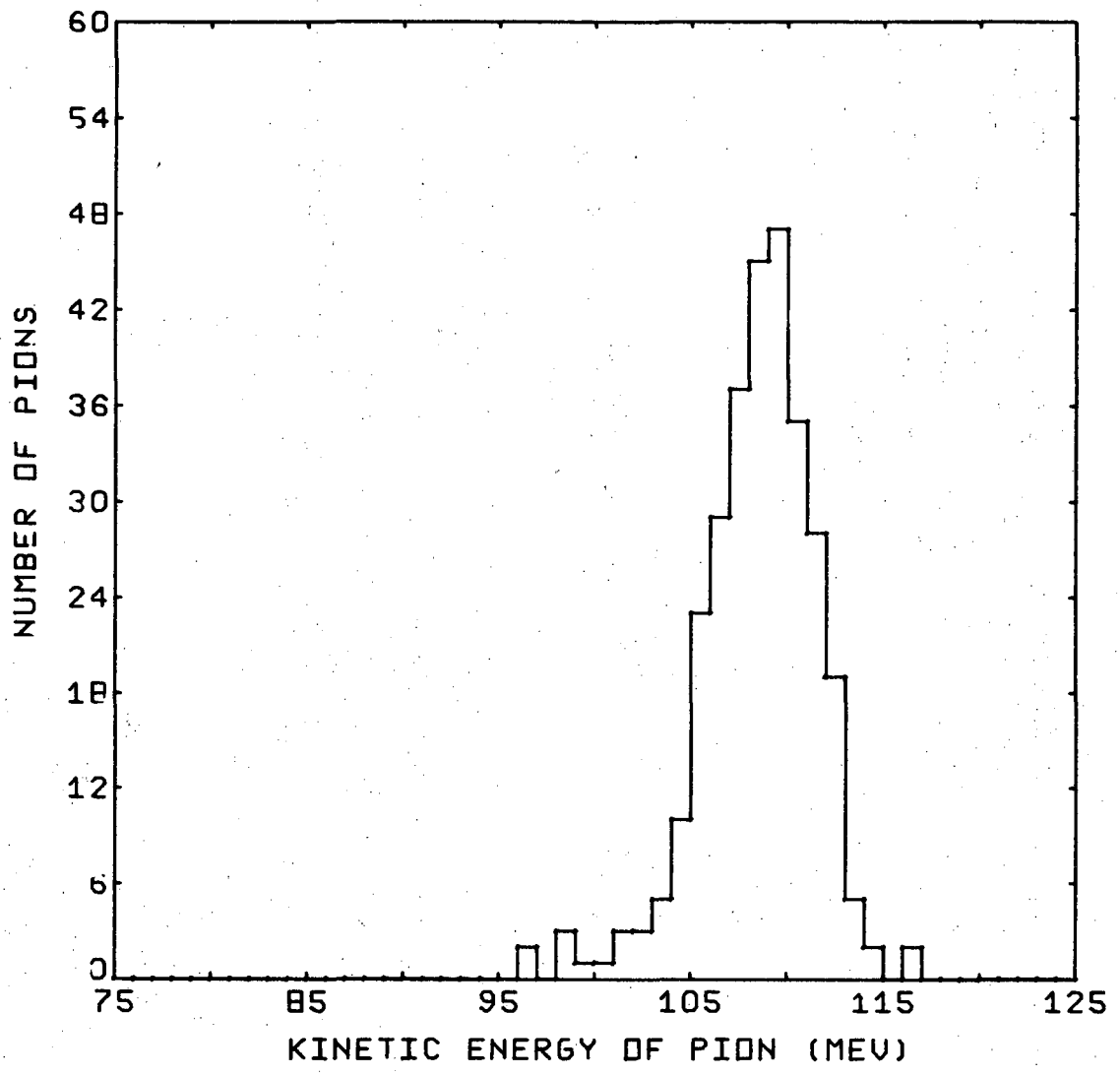


XBL 6812-6343

Fig. 21. Distribution in the kinetic energy of the $\pi^+$ in a sample of $K^+ \rightarrow \pi^+ + \pi^o$ events.

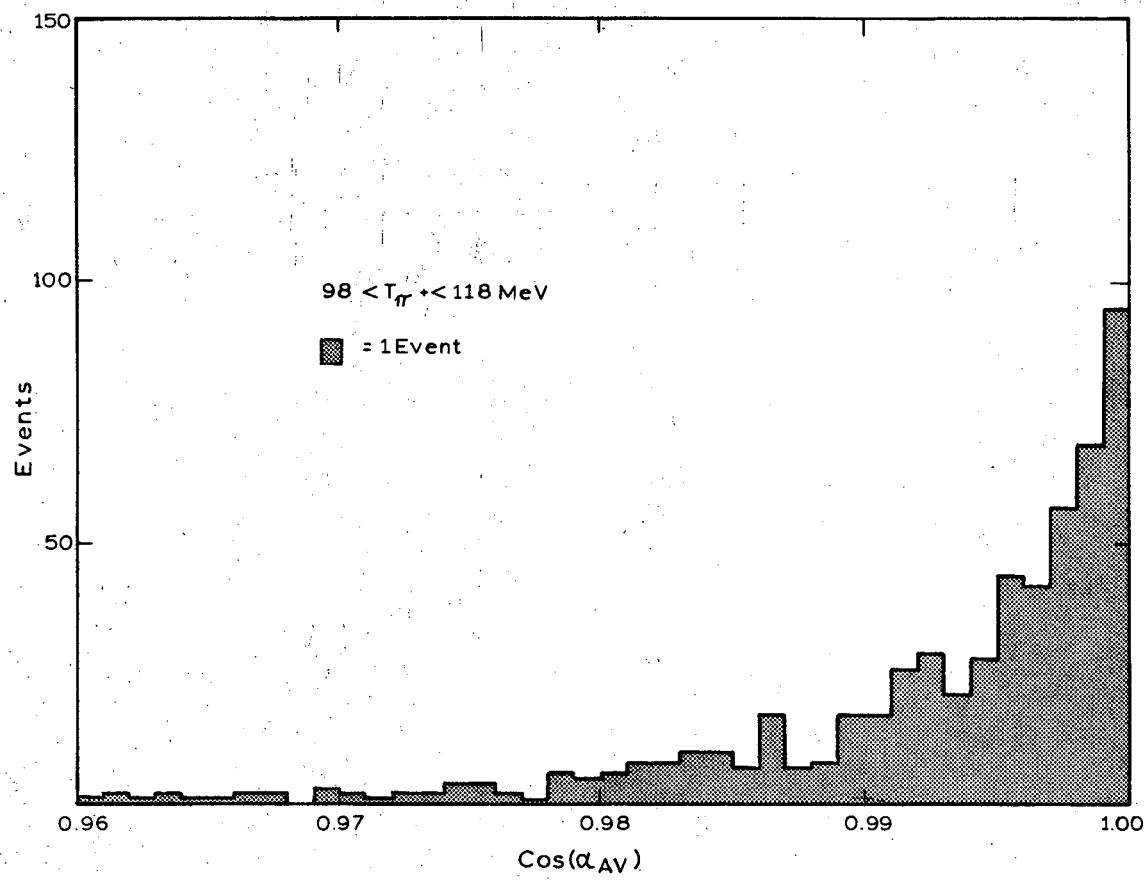


XBL 670 2098

Fig. 22. Distribution in cos $\alpha_{av}$ of a sample of $K^+ \rightarrow \pi^+ + \pi^o$ events. $\alpha_{av}$ is the averaged angle between the measured and the predicted direction of one of the gamma rays in the decay $K^+ \rightarrow \pi^+ + \gamma + \gamma$.

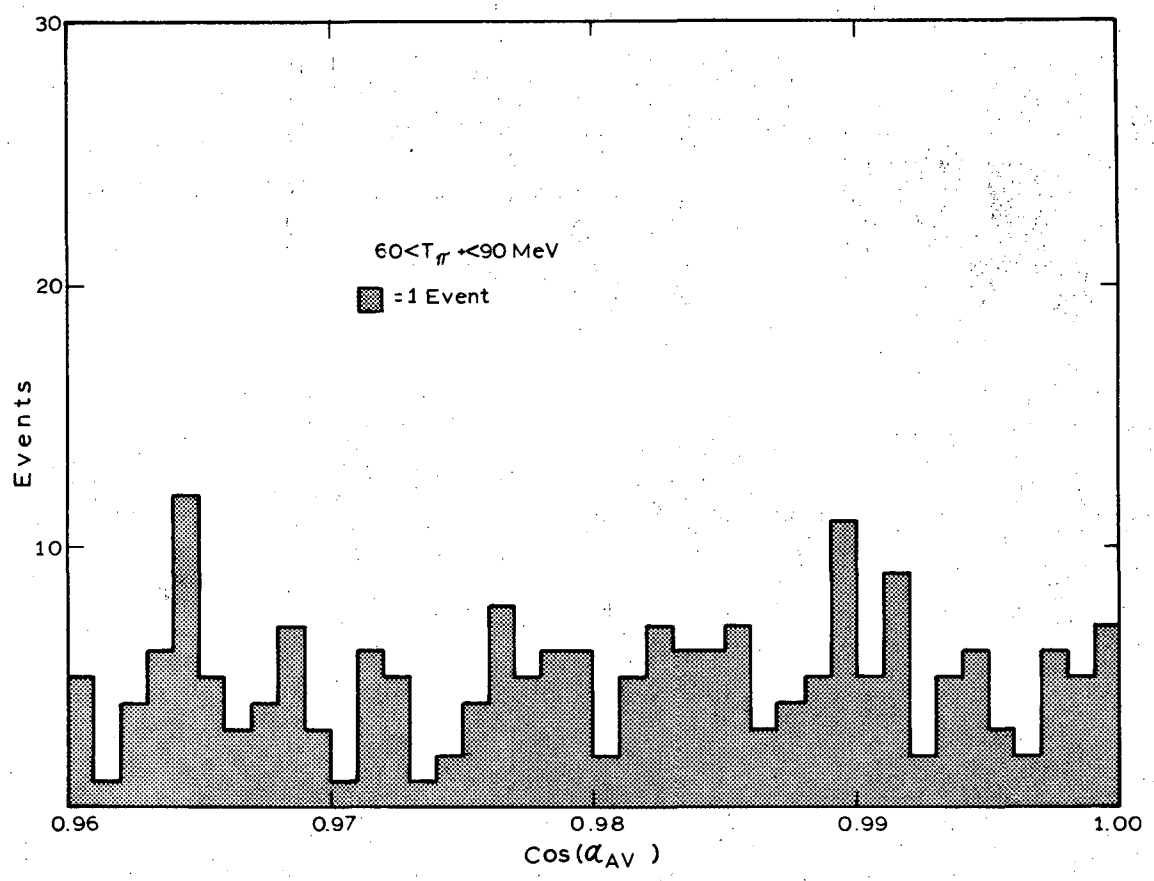


XBL 670 2099

Fig. 23. Distribution in cos $\alpha_{av}$ of the sample of the $K^+$ decay events in which we searched for examples of the reaction $K^+ \rightarrow \pi^+ + \gamma + \gamma$ with the invariant mass of the two gamma rays not equal to the $\pi^o$ mass. Our upper limit on the branching ratio for this mode comes from the conclusion that there are fewer than 11 events in the interval from 0.994 to 1.0.

where $\lambda$ is a constant,

(2) Off-mass-shell model, i.e. assuming the distribution to be of the form of Eq. (II-7).

(3) $\sigma$ meson intermediate state model, i.e. assuming the distribution function:

$$\frac{d\Gamma(K^+ \to \pi^+ + \gamma + \gamma)}{dE_{\pi^+}} = \lambda \frac{P_{\pi^+} q^4}{(q^2 - m_\sigma^2 + \frac{\Gamma_\sigma^2}{4})^2 + m_\sigma^2 \Gamma_\sigma^2} \qquad \text{(II-10)}$$

$m_\sigma$ is the mass of the $\sigma$, assumed to be 400 MeV, and $\Gamma_\sigma$ is its width, assumed to 100 MeV. $\lambda$ is a constant.

(4) $\epsilon$ meson intermediate state model, similar to the $\sigma$ meson model but with $M_\sigma = 700 + i50$ MeV.

The purposes of these calculations were as follows:

(1) To calculate the detection efficiencies of the charged pion and the two gamma rays for the decay $K^+ \to \pi^+ + \gamma + \gamma$ corresponding to different distribution functions.

(2) To determine the effect of measurement error on the predicted second photon direction.

The result of the calculation is shown in Table IV.

Table IV. Results of Monte Carlo calculation.

| | Phase space model | Off-mass-shell model | σ meson model | Calibrating data with $K^+_{\pi 2}$ |
|---|---|---|---|---|
| Spectrum accepted | | | | |
| Degrader I | 19.2% | 13.0% | 5.6% | 100% |
| Degrader II | 17.7% | 15.8% | 9.2% | |
| Detection efficiency of the two gammas | 33.0% | 32% | 32% | 50% |
| Loss due to π-nucleus scattering | 23% | 23% | 23% | 40% |

The possible measurement errors of the charged pion energy and the directions of gamma ray showers were estimated from the $K_{\pi 2}$ data:

(1) The energy measurement error was directly read from the $K_{\pi 2}$ spectrum curve to be ±4 MeV which is mainly due to the range uncertainty because of the straggling of the pion through material.

(2) Taking the pion energy of the $K_{\pi 2}$ events to be 108.6 MeV we calculated the angular measurement errors of the gamma rays to be less than 0.077 radian from the new cos $\alpha_{av}$ plot in Fig. 24.

The uncertainty in the pion energy measurement was estimated to be smaller for the 60 to 90 MeV pions than for the 108.6 MeV pions. However in order to cover any unknown systematic error, we used ±5 MeV as the energy measurement uncertainty in analyzing the data. The angular measurement error of the gamma ray is the same for $K_{\pi 2}$ events and the $K_{\pi\gamma\gamma}$ data. Therefore we believe it is safe to use the above energy

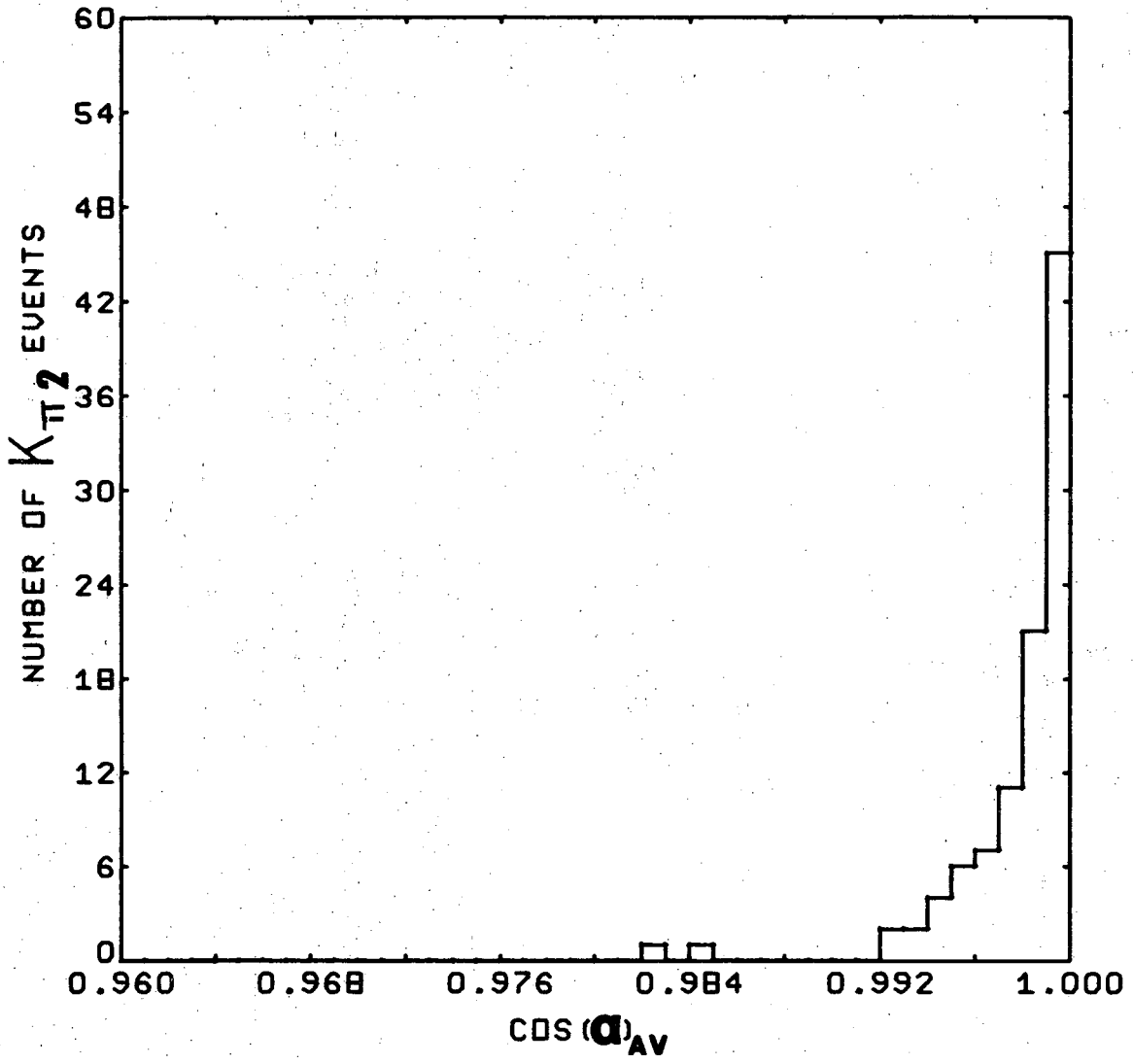


XBL 6812-6338

Fig. 24. Distribution in cos $\alpha_{av}$ of a sample of $K^+ \rightarrow \pi^+ + \pi^o$ events if we assume $E_\pi$ = 108.6 MeV. The deviation from the line cos $\alpha_{av}$ = 1 is due to the measurement errors in the directions of the pion and gamma rays.

and angular errors in calculating the resolution curve of the fake $K_{\pi\gamma\gamma}$ events in the cos $\alpha_{av}$ plot in Fig. 25.

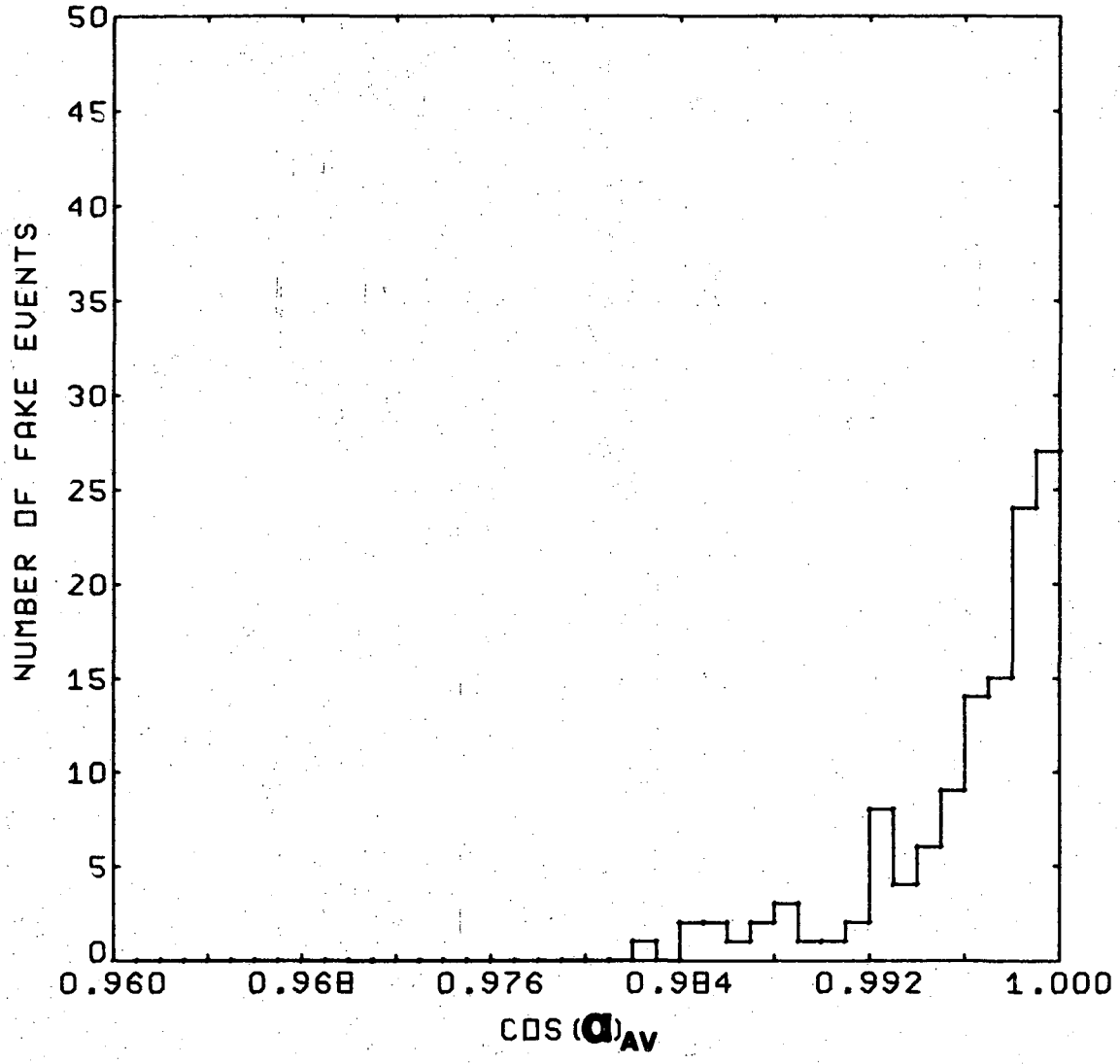


XBL 6812-6339

Fig. 25. Distribution in cos $\alpha_{av}$ of fake $K^+ \rightarrow \pi^+ + \gamma + \gamma$ events with $60 < E_\mu < 90$ MeV.

## E. RESULTS

The simplest way of displaying the experimental results is to compare the cos $\alpha_{av}$ curves in Fig. 22, Fig. 23, and Fig. 25 with each other. In Fig. 22 we see that 61% of the $K_{\pi 2}$ events are distributed in the interval $0.994 < \cos \alpha_{av} < 1.000$. The distribution curve of the fake $K_{\pi\gamma\gamma}$ events is shown in Fig. 25, where we have used the same uncertainties in pion energy measurement and gamma-ray angular measurement we calculated from the $K^+ \rightarrow \pi^+ + \pi^o$ data.

We found 80% of the $K_{\pi\gamma\gamma}$ events should lie in the interval $0.994 < \cos \alpha_{av} < 1.000$. In general the resolution in cos $\alpha$ gets better when the pion energy decreases for $K_{\pi\gamma\gamma}$ events. Figure 23 shows the distribution in cos $\alpha_{av}$ of our data with the pion energy between 60 and 90 MeV. The uniformly distributed events are mainly $K^+ \rightarrow \pi^o + \nu + \mu^+$ events. As a check we generated $K_{\mu 3}$ events according to the distribution in the Dalitz plot calculated from V-A theory and from the assumption that the effect of the term with the form factor $F_-$ is negligible.

The pion energy was then calculated from the range of the muon with given muon energy. Figure 26 shows the distribution of the generated $K_{\mu 3}$ events in cos $\alpha_{av}$. We see the distribution is uniform in the interval $0.96 < \cos \alpha_{av} < 1.00$ consistent with the distribution of the data. We have used the number of observed background events in the interval $0.96 < \cos \alpha_{av} < 0.99$ to predict the number of background events expected in the interval $0.994 < \cos \alpha_{av} < 1.000$. We predicted $30 \pm 3$ events. We observed 29 events in this interval. The excess of the observation over the prediction is $-1 \pm 6$ events. At the 90% confidence level we concluded that there are fewer than 11 events in

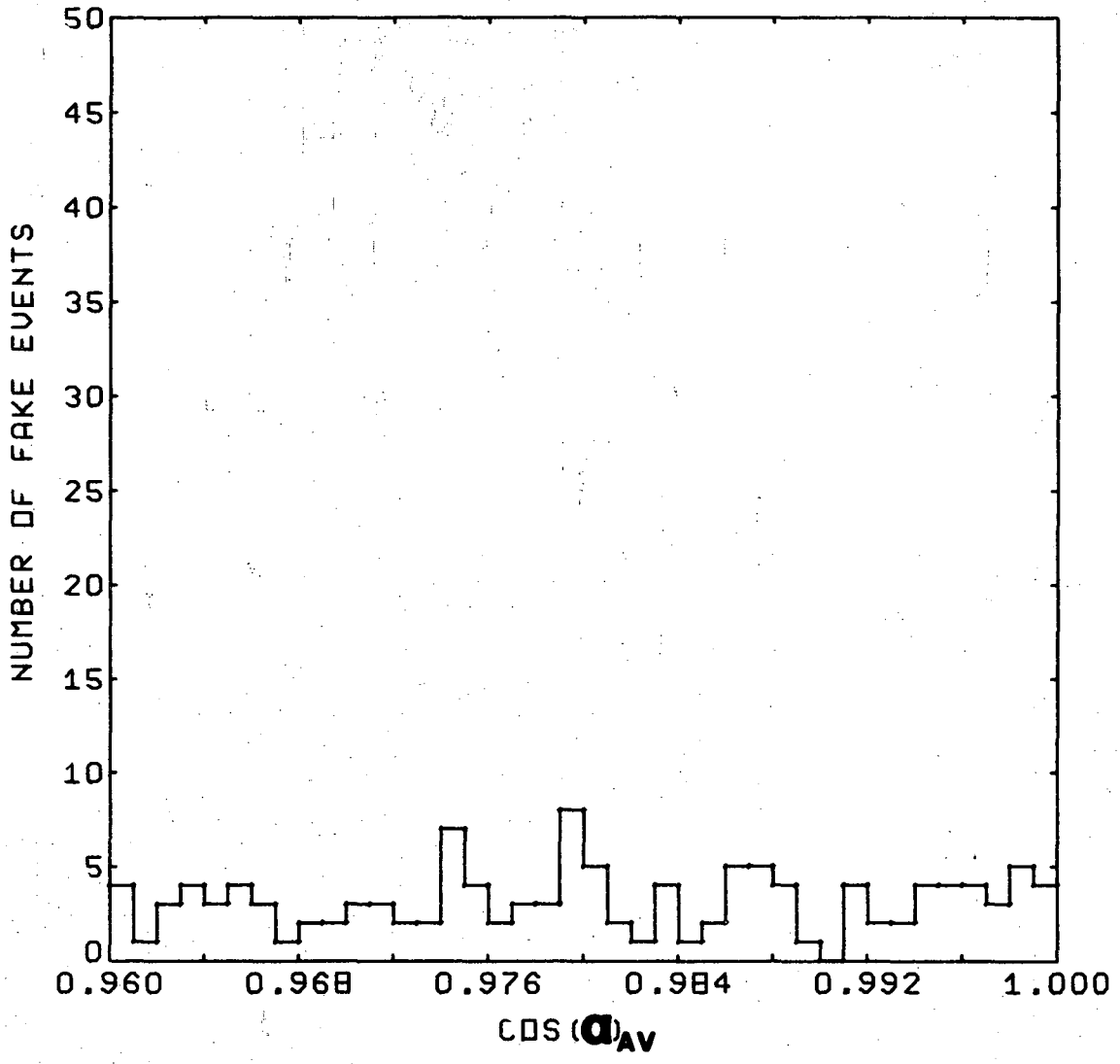


XBL 6812-6337

Fig. 26. Distribution in cos $\alpha_{av}$ of fake $K^+_{\mu 3}$ events with $55 < E_\mu < 81$ MeV.

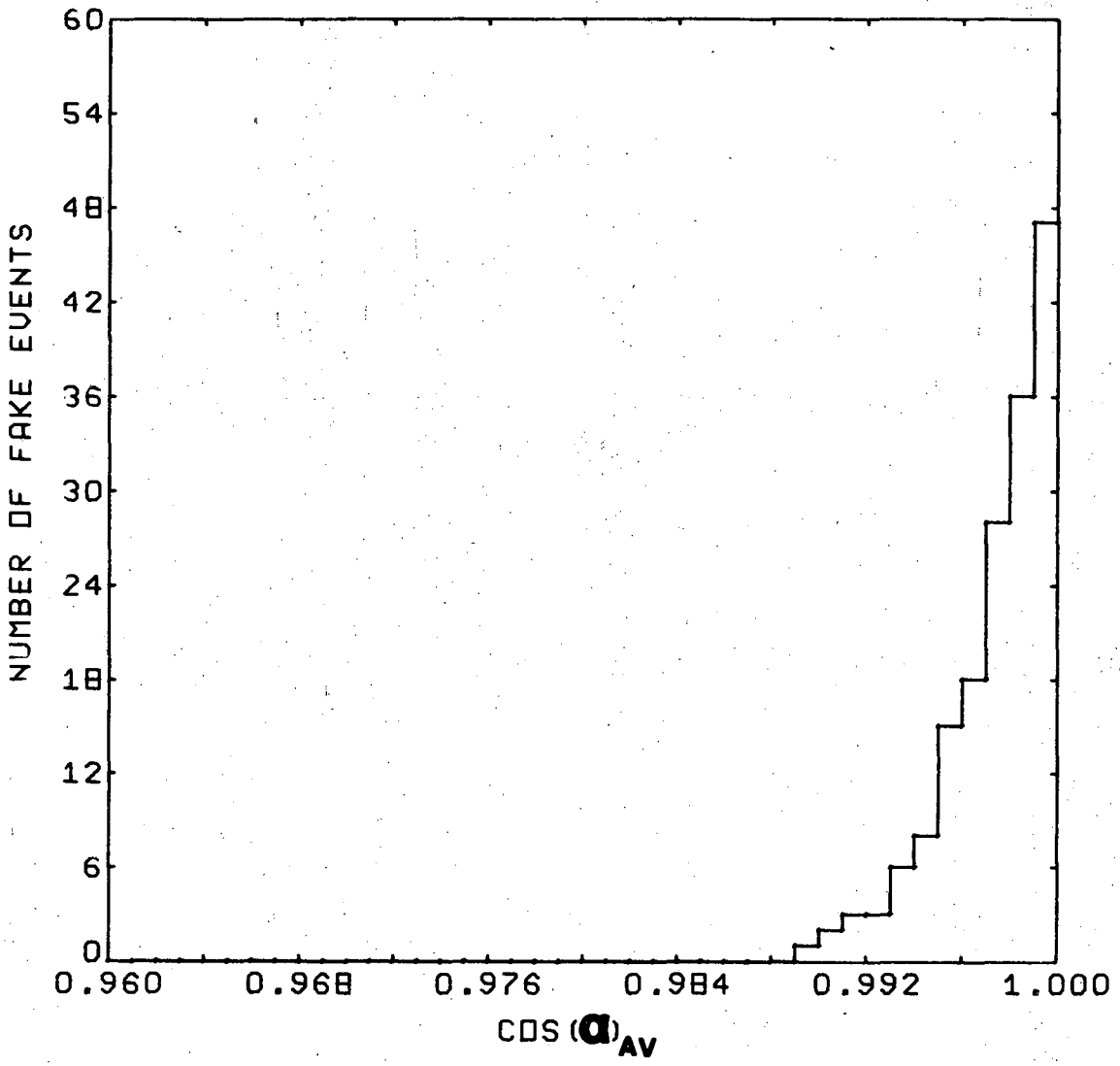


XBL 6812-6336

Fig. 27. Distribution in cos $\alpha_{av}$ of fake $K^+_{\pi 2}$ events if the measurement in $E_{\pi^+}$ were perfect. The uncertainty in measuring the pion and gamma ray angles is assumed to be 0.077 radians.

the interval $0.994 < \cos \alpha_{av} < 1.000$. This gives an upper limit of $1.5 \times 10^{-4}$ for charged pions with kinetic energy less than 90 MeV if the decay occurs according to the differential distribution of Eq. (II-7).

As a final check on our efficiency calculation, we have calculated the $K_{\pi 2}$ branching ratio from the $K_{\pi 2}$ sample. In one sample of our $K_{\pi 2}$ data we observed 18270 delayed $K^+$ decay defined by Eq. (II-8). After various losses in the data reduction we were left with 9542 delayed $K^+$ decays. The loss due to pion nucleus interaction was estimated to be 0.4. The detection probability of the two gamma rays was calculated by the Monte Carlo program to be 0.5. There were 366 $K_{\pi 2}$ events in the interval $0.996 < \cos \alpha_{av} < 1.00$ while 60% of the $K_{\pi 2}$ events were expected to be in this interval. From this we find the branching ratio of $K_{\pi 2}$ to be 19% which agrees quite well with the accepted value 20.84% in the table[21] of Rosenfeld et al.

We would like to consider the significance of our result. The upper limit on the branching ratio with pion energy between 70 and 90 MeV is $2 \times 10^{-5}$ corresponding to a 90% confidence level. The average value of the differential spectrum relative to $K^+_{\pi 2}$ branching ratio is $5 \times 10^{-6}$ for the energy interval 70 to 90 MeV. As can be seen from Fig. 20, this corresponds to an upper limit on $\xi$ of 30, and to a rate for all charged pions of energy less than 90 MeV of approximately three times that predicted by Fujii's model ($\xi \approx 20$ , but with newer $\pi^o$ lifetime). There are at least two ways to improve our measurement:

(1) One can reajust the degrader to allow less energetic pions (say between 55 to 70 MeV) to stop inside the pion range spark chamber. The resolution curve gets better for pions with lower energy and one

can get a bigger portion of the $K^+ \to \pi + \gamma + \gamma$ spectrum.

(2) One can also replace the pion range spark chamber with a stack of scintillation counters. After the pion stopped in a certain counter, one can require a delayed (say 10 ns after the pion stopped) second pulse coming from the same counter. By requiring this $\pi \to \mu$ decay, one can reject the number of the muons from $K_{\mu 3}$ by a factor of at least 100. We note that $K_{\mu 3}$ was the main background in this experiment.

With respect to the $\sigma$ meson intermediate state model, our result, which is relatively insensitive to the assumed $\sigma$ meson parameters, is that if the $K^+ \to \pi^+ + \gamma + \gamma$ decay proceeds via a $\sigma$ meson intermediate state, the total branching ratio of the $K^+$ meson into this channel is less than $3.3 \times 10^{-4}$. This is more than an order of magnitude lower than the prediction of the Lapidus model. We would like to point out, however, that the $\sigma$ intermediate state model would not be in disagreement with our results if the ratio, r, of the decay modes $\eta_o \to \pi^o+\gamma+\gamma$ to $\eta_o \to 3\pi^o$ were more than an order of magnitude smaller than the predicted[15] value 0.3. The present experimental results[21] indicate $r=0.12 \pm 0.1$ which is consistent with both zero and the predicted value 0.3.

Various other $0^+$ meson intermediate state models have been considered in the literature. Oneda[24] suggested an $\epsilon$ model ($m_\epsilon$ = 700 MeV). For this model our results limit the total branching ratio to be less than $1.8 \times 10^{-4}$.

Finally, if we assume that the hypothetical $K^+ \to \pi^+ + \gamma + \gamma$ decay is governed by a phase space model, that is, if the distribution of the $\pi^+$ is as follows

$$\frac{d\Gamma(K^+ \to \pi + \gamma + \gamma)}{dE_\pi} = \lambda \, P_{\pi^+}$$

where $\lambda$ is a constant, our experimental result limits the total branching ratio of the $K^+$ into this mode to be less than $1.1 \times 10^{-4}$ or the partial decay rate less than $1.0 \times 10^4$ sec$^{-1}$.

The experimental situation of the measurements on the branching ratio of $K_2^o \to \pi^o + \pi^o$ is very confusing.[31] One possibility of this confusion is that the branching ratio $K_2^o \to \pi^o + \gamma + \gamma$ might be quite large thus different methods of measurement of the decay rate $K_2^o \to \pi^o + \gamma + \gamma$ might accept different amount of $K_2^o \to \pi^o + \gamma + \gamma$ and get different results. Assuming the decay rate $K^+ \to \pi^+ + \gamma + \gamma$ is of the same order as $K_2^o \to \pi^o + \gamma + \gamma$, we can set an upper limit for the decay rate of $K_2^o \to \pi^o + \gamma + \gamma$ of $10^4$ sec$^{-1}$ or the branching ratio of $K_2^o \to \pi^o + \gamma + \gamma$ of $5 \times 10^{-4}$ which is smaller than the observed $K_2^o \to \pi^o + \pi^o$ branching ratio (about 2 to $4 \times 10^{-3}$). We therefore concluded that if the above assumption is reasonable then the decay $K_2^o \to \pi^o + \gamma + \gamma$ will not affect the rate $K_2^o \to \pi^o + \pi^o$ or $\eta_{oo}$ which was defined as

$$\eta_{oo} = \frac{\tau(K_2^o \to \pi^o \pi^o)}{\tau(K_2^o \to \pi^+ \pi^-)} \quad .$$

REFERENCES

1) J. Bernstein, G. Feinberg and T. D. Lee, Phys. Rev. 139, B1650 (1965)

2) N. Cabibbo, Nuovo Cimento IL, Vol. XI, N.6, p. 837, (1959).

3) D. E. Neville, Phys. Rev. 124, p. 2037 (1961).

4) J. L. Gervais, J. Ilipoulos and J. M. Karplan, Phys. Letters 20, 432 (1966).

5) A. Q. Sarker, Phys. Rev. 173, 5, p. 1749 (1968).

6) T. D. Lee and C. N. Yang, Phys. Rev. 119, 1410 (1959), Phys. Rev. Letters 4, 307 (1960).

E. S. Ginsberg and R. H. Pratt, Phys. Rev. 130, 5, p. 2105 (1963).

7) R. Burns et al., Phys. Rev. Letters 15, p. 42 (1965).

8) M. Deutsch, Proceedings of the Conference on Photon Interactions in the Bev-Energy Range (Jan. 1963) VII. 18.

9) R. R. Wilson, Phys. Rev. 84, 100 (1951); Phys. Rev. 86, 261 (1952).

10) J. W. Cronin et al., The Review of Scientific Instruments Volume 33, 9, p. 946 (1962).

11) V. S. Vanyashin et al., JINR-P1-3594 (1967).

12) J. D. Jackson, Private Communication.

13) M. Gell-mann and A. Pais, Proceeding of the 1954 Glasgow Conference on Nuclear and Meson Physics (Pergamon Press, New York, 1955).

14) Y. Fujii, Phys. Rev. Letters 17, 613 (1966).

15) I. Lapidus, Nuovo Cimento 46, 668 (1966).

16) Y. Fujii, Private Communication.

17) N. Cabibbo and R. Gatto, Phys. Rev. Letters 5, 382 (1960).
S. Oneda, Y. S. Kim and D. Korff, Phys. Rev. 136, B1064 (1964).

18) Y. Hara and Y. Nambu, Phys. Rev. Letters 16, 875 (1966).

19) S. Okubo, R. E. Marshak, and V. S. Mathur, UR-875-200, University of Rochester, Department of Physics and Astronomy.

20) D. Cline and W. Fry, Phys. Rev. Letters 13, 101 (1964).

21) Barash-Schmidt, Barbaro-Galtieri, Podolsky, Price, Rosenfeld, Soding, Wohl and Roos, UCRL-8030 (August 1968).

22) L. Brown and P. Singer, Phys. Rev. 133, B812 (1964).

23) L. Brown, "Scalar Mesons" in Perspectives in Modern Physics, ed. by R. Marshak, Wiley, 1966, pp 195 - 210.

24) S. Oneda, Phys. Rev. 158, 1541 (1967).

25) G. Oppo and S. Oneda, Phys. Rev. 160, 1397 (1967).

26) Fäldt, Peterson, and Pilkuhn, Nuclear Physics B3, pp 234-240 (1967).
K. L. Kowalski and J. Eshelman, Case Western Reserve University, Nuclear Physics Laboratory Progress Report, Coo-1573-33 (1967).

27) Y. Hara, Tokyo University Preprint, TUEP-66-17.

28) J. J. Sakurai, Vector Meson Dominance and Current Algebra, pp 81-91 of Proceeding of the Fifth Annual Eastern Theoretical Physics Conference, Brown University. Feldman, David (ed.) W. A. Benjamin, Inc. (1967).

29) F. Selleri, to be published in Nuovo Cimento.

30) N. Cabibbo, Proceeding of the 13th. International Conference on High Energy Physics at Berkeley, pp 31, (1966).

31) 14th International Conference on High Energy Physics at Vienna (August 1968).

32) D. Friedell et al., MIT-2098-389.

33) Tannenbaum, Russell and Sah, Proceeding 1967 International Symposium on Electron and Photon Interactions at High Energies (1967) pp 519.

34) T. Devlin, Phys. Rev. Letters 20, 638 (1968).

ACKNOWLEDGMENTS

The author is deeply grateful to Professor Emilio Segrè for his guidance and encouragement. He would also like to thank:

Dr. Rae F. Stiening for his introducing him into the experimental high energy physics without whom this thesis is totally impossible;

Professor John David Jackson for clarifying many theoretical ideas and for his critical reading over this thesis;

Dr. Clyde Wiegand who designed and supervised the construction of most of the equipment used in both experiments;

Professor Gordon Struble for reading over this thesis;

Professor Martin Deutsch whose automatic scanning device greatly speeded up the reduction of the date;

Dr. David Cutts whose thesis experiment produced the film used in the second part of the thesis ($K^+ \to \pi^+ + \gamma + \gamma$) and for his efforts in the design of beam, scanning and programming;

Dr. Peter Kijewski for many helpful discussions and Dr. Raymond Kunselmann for his reading over this thesis;

Mrs. Rosemary Fowell for her assistance with the manuscript;

The United States Atomic Energy Commission for the financial support of this experiment.

This work is dedicated to Suzanne.

APPENDIX A

## $\Delta I = 1/2$ Rule for K Meson Hadronic and Semi-Leptonic Weak Decay Modes

Isotopic spin is conserved in strong interactions but not in electromagnetic or weak interactions. Since the isotopic spin of the K meson is 1/2, the $\Delta I = 1/2$ rule for weak interactions requires the total isotopic spin of the final state of any K meson decay mode to be 0 or 1. The $\Delta I = 1/2$ rule is generally well obeyed for the K-meson hadronic and semi-leptonic decay modes. The deviation from the predicted values based on $\Delta I = 1/2$ rule is less than 10%. The small deviation can be either attributed[30] to:

1) corrections due to electromagnetic interactions, or

2) the existence of some $\Delta I = 3/2, 5/2, \ldots$ weak interaction amplitudes which are much smaller than the $\Delta I = 1/2$ amplitude.

The electromagnetic corrections usually are of the order of 1/137 but in some cases the corrections can be as large as 1/20. One example where the correction is large is the mass splitting of the pi mesons:

$$(m_{\pi^+} - m_{\pi^0})/m_{\pi^+} \approx 5/140 \approx 1/28 \ .$$

We have listed below some of the relations among K meson decay modes as predicted by the $\Delta I = 1/2$ rule. The predicted values are compared with most recent experimental results based on the papers submitted to the 14th International Conference on High Energy Physics, Vienna 1968, whenever applicable and otherwise with the decay rates summarized in the Table of Rosenfeld et al. (August 1968).

| | Ratio of various decay modes | Ratio predicted by $\Delta I = 1/2$ rule | Phase space correction | Experimental data | Remark |
|---|---|---|---|---|---|
| 1. | $\frac{R(K^+ \to \pi^+ + \pi^0)}{R(K^0 \to \pi^+ + \pi^-)}$ | 0 | | $\frac{1}{450}$ | (a) |
| 2. | $\frac{R(K_1 \to \pi^0 + \pi^0)}{R(K_1 \to \pi^+ + \pi^-)}$ | $\frac{1}{3}$ | small | $0.316 \pm 0.011$ | O.K. |
| 3. | $\frac{2R(K^+ \to \pi^0 + \mu^+ + \nu)}{R(K_2^0 \to \pi^\mp + \mu^\pm + \nu)}$ | $\frac{1}{1}$ | small | $\frac{1}{1.05 \pm 0.05}$ | O.K. |
| 4. | $\frac{2R(K^+ \to \pi^0 + e^+ + \nu)}{R(K_2^0 \to \pi^\pm + e^\mp + \nu)}$ | $\frac{1}{1}$ | small | $\frac{1}{0.99 \pm 0.04}$ | O.K. |
| 5. | $\frac{R(K_2^0 \to \pi^0 + \pi^0 + \pi^0)}{R(K_2^0 \to \pi^+ + \pi^- + \pi^0)}$ | $\frac{3}{2}$ | $\times \frac{1.495}{1.225} = 1.83$ | $1.67 \pm 0.07$ | O.K. |
| 6. | $\frac{R(K_2^0 \to \pi^+ + \pi^- + \pi^0)}{R(K^+ \to \pi^+ + \pi^0 + \pi^0)}$ | $\frac{2}{1}$ | $\times \frac{1.225}{1.245} = 1.98$ | $1.78 \pm 0.06$ | (b) |
| 7. | $\frac{R(K_2^0 \to \pi^0 + \pi^0 + \pi^0)}{R(K^+ \to \pi^+ + \pi^+ + \pi^-)}$ | $\frac{3}{4}$ | $\times 1.49 = 1.1$ | $0.90 \pm 0.06$ | (c) |

(a) The $\Delta I = 1/2$ rule is apparently violated. However the ratio is only of the order of $(1/20)^2$. It was suggested by Cabibbo that the decay $K^o \rightarrow 2\pi$ is forbidden in the limit of $SU_3$ symmetry and it is likely that the rate is one order of magnitude smaller than what would be if it were not forbidden. Therefore it is possible to attribute the violation of the $\Delta I = 1/2$ to electromagnetic corrections of weak decays.

(b) As was pointed out by Devlin[34] that there is a $\pm 10\%$ uncertainty in the predicted value of this ratio based on the $\Delta I = 1/2$ rule due to some uncertainty in determining the centers of the Dalitz plots.

(c) This ratio appears to be inconsistent with the $\Delta I = 1/2$ rule. However the ratio of the $\Delta I = 3/2$ amplitude needed to account for the inconsistency to the $\Delta I = 1/2$ amplitude is still of the same order as that in a.

APPENDIX B

## Experimental Evidence of the Conservation of Angular Momentum for Weak Interactions

After the discovery of the violation of the symmetry laws C, P and CP in weak decays, it becomes advisable to test the validity of other conservation laws such as the rule that any integer or half integer spin particle must obey Bose or Fermi statistics and the conservation of angular momentum. The former is still under investigation for muon.[33] There seems to be no direct experimental evidence that the rule is valid for K mesons or other strange particles. The conservation of angular momentum is commonly believed to be guaranteed by Lorentz invariance. Since there are so many examples of Lorentz invariance in weak interactions the conservation of angular momentum is usually taken to be established in weak interactions.

It was shown by Franco Selleri[29] that Lorentz-invariance does not necessarily lead to angular momentum conservation, if one introduces some fairly daring hypothesis. His mechanism for angular momentum violation is to assume existence of a particle (spurion) with spin, but with zero four-momentum. This particle would appear in weak interaction strangeness changing reactions. Therefore the angular momentum of detectable particles in weak interaction reactions would not be conserved while their energy and momentum would be strictly conserved.

Observing that the spins of the strange particles K, $\Lambda$, $\Sigma$, $\Xi$ have not been measured directly but have been deduced from the assumptions of total angular momentum conservation, Selleri claimed that several new sets of assignment of spins for strange particles corresponding to

different spin values for his spurion, would be consistent with the present experimental evidence.

If the spin of the spurion were 1/2, Selleri's assignments of spin for strange particles would be:

| K | $\Lambda$ | $\Sigma$ | $\Xi$ |
|---|---|---|---|
| 1/2 | 1 | 1 | 3/2 |

with selection rules $\Delta I = 1/2$, $\Delta J = 1/2$.

If the spin of the spurion were 1, his assignments would be:

| K | $\Lambda$ | $\Sigma$ |
|---|---|---|
| 1 | 3/2 | 3/2 |

with selection rules $\Delta I = 1/2$, $\Delta J = 1$.

In either of the above schemes, he claims that the new assignments have theoretical advantages over the conventional assignments while both assignments are consistent with the present experimental data.

Some of the theoretical advantages are:

1. The $\Delta I = 1/2$ rule becomes rigorous in weak interactions.
2. Strangeness conservation in e.m. interactions becomes a consequence of J-conservation.
3. The $\Delta S = 1$ rule becomes a consequence of the $\Delta I = 1/2$ rule.

The weakness of these schemes lies in the assumption of an unobservable particle--spurion, and in the contradiction with the success of the SU(3) scheme. The direct measurements of the spins of the strange particles would prove or disprove this scheme of J-violation, however the experimental measurements are very difficult to carry out. We would like to point out here an experimental result on the upper limit of the decay $K^+ \to \pi^+ + \gamma$ of $5.6 \times 10^{-5}$ measured by Friedell et al.[32] as an indirect evidence against the J-violation scheme. We observe that if

the K meson had spin 1/2 (or 1) and the selection rule in strangeness changing weak interactions were $\Delta I = 1/2$ and $\Delta J = 1/2$ (or $\Delta J = 1$), the decay reaction $K^+ \to \pi^+ + \gamma$ would be allowed in either set of the new spin assignments. Further from the simple Feynman diagrams,

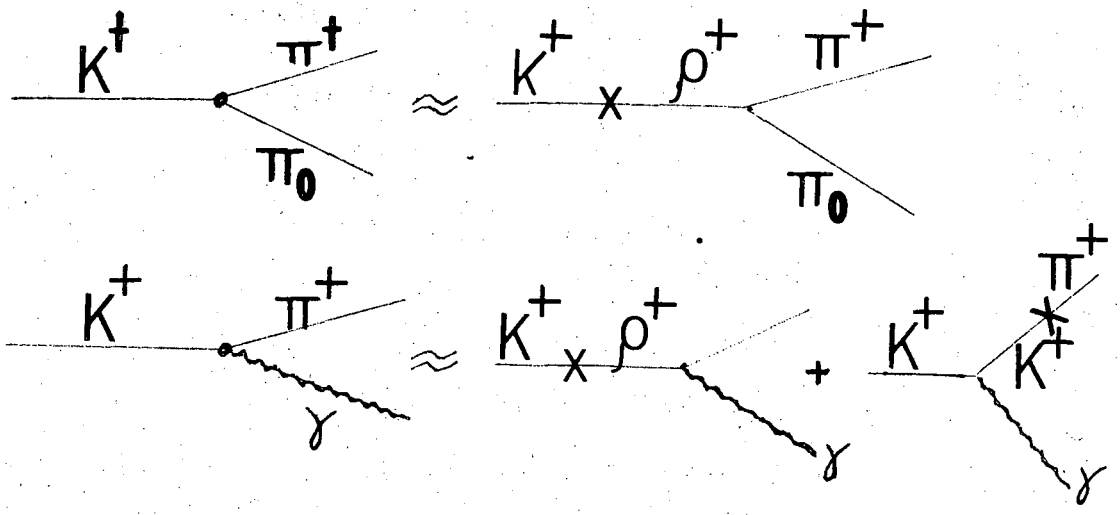


where × means the decay due to weak interaction, we can estimate that with the new spin assignments, the branching ratio of $K^+ \to \pi^+ + \gamma$ would be of the order of $10^{-3}$ if the coupling constant $f_{\pi K}$ is not otherwise suppressed compared with $f_{\rho K}$. This is an order of magnitude higher than the experimental upper limit. Therefore we have here an experimental evidence against the existence of a spurion with nonzero angular momentum but zero four momentum in weak interactions. Only if the $\pi K$ coupling constant is unexpectedly suppressed, then the branching ratio of $K^+ \to \pi^+ + \gamma$ could drop to $10^{-4}$, comparable to the experimental upper limit.

## LEGAL NOTICE

*TECHNICAL INFORMATION DIVISION*
*LAWRENCE RADIATION LABORATORY*
*UNIVERSITY OF CALIFORNIA*
*BERKELEY, CALIFORNIA 94720*